[American Journal of Science, Vol. 321, March, 2021, P. 365–391, DOI 10.2475/03.2021.03]

$^{40}Ar/^{39}Ar$ AND LA-ICP-MS U–Pb GEOCHRONOLOGY FOR THE NEW ENGLAND PORTION OF THE EARLY CRETACEOUS NEW ENGLAND-QUEBEC IGNEOUS PROVINCE: IMPLICATIONS FOR THE POSTRIFT EVOLUTION OF THE EASTERN NORTH AMERICAN MARGIN

JENNIFER R. COOPER BOEMMELS*,**,†, JEAN M. CRESPI**,
LAURA E. WEBB***, and JULIE C. FOSDICK**

ABSTRACT. The Early Cretaceous New England-Quebec igneous province is a classic example of postrift magmatism along the eastern North American passive margin. Although a suite of $^{40}Ar/^{39}Ar$ ages has been available for the Monteregian Hills lobe in the Quebec portion of the New England-Quebec igneous province for many years, only a single high accuracy radiometric age has been published for the Burlington lobe and none for the Taconic lobe in the New England portion of the province. As a result, the timing of and driving mechanisms behind the magmatism have remained unresolved, and a hotspot origin for the entire province persists in the literature. We have dated four dikes and one pluton in the Burlington and Taconic lobes using $^{40}Ar/^{39}Ar$ and U–Pb geochronology to improve understanding of the age of magmatism in the New England portion of the province. In the Burlington lobe, $^{40}Ar/^{39}Ar$ plateau ages include a 137.55 ± 1.80 Ma biotite age and a 136.9 ± 4.2 Ma amphibole age for a lamprophyre dike from Charlotte, Vermont, and a 133.6 ± 2.2 Ma biotite age for a lamprophyre dike from Colchester, Vermont. In the Taconic lobe, ages include an $^{40}Ar/^{39}Ar$ plateau amphibole age of 107.09 ± 1.32 Ma for a lamprophyre dike from Castleton, Vermont, a 122 Ma minimum $^{40}Ar/^{39}Ar$ biotite age for a lamprophyre dike from Poultney, Vermont, and a 103.13 ± 0.53 Ma LA-ICP-MS U–Pb zircon age from the quartz syenite of the Cuttingsville complex. These results show that magmatism spanned at least 35 Ma, from ~138 to 103 Ma, which is broadly consistent with the span of magmatism suggested by workers in the 1970s and 1980s based on K–Ar and Rb–Sr ages. This extended span of magmatism for the Burlington and Taconic lobes is in contrast to the brief 1 to 2 Ma episode of magmatism at ~124 Ma inferred for the Monteregian Hills lobe. The New England-Quebec igneous province has traditionally been attributed to passage of the Great Meteor hotspot. However, given the close proximity of the Burlington and Taconic lobes, the magmatism in these lobes should span only a few Ma if the product of a hotspot. The age data are also difficult to reconcile with a more complex expression of hotspot magmatism in continental lithosphere related to either plume head magmatism or long-distance migration of plume material. Instead, the extended duration of Early Cretaceous New England-Quebec igneous province magmatism in New England may represent an expression of edge-driven convection, a process known to occur along passive margins and inferred to be operating beneath the eastern North American margin today.

Key words: passive margin, postrift magmatism, eastern North American margin, New England-Quebec igneous province, Great Meteor hotspot

INTRODUCTION

Passive margin development is a complex and long-lived process that continues well beyond rifting and the initial establishment of a passive margin setting (Praeg and others, 2005; Mazza and others, 2014, 2017; Amidon and others, 2016). Following

* Department of Earth Science, Southern Connecticut State University, New Haven, Connecticut 06515–1355
** Department of Geosciences, University of Connecticut, Storrs, Connecticut 06269–1045
*** Department of Geology, University of Vermont, Burlington, Vermont 05405–1758
† Corresponding author: cooperj1@southernct.edu

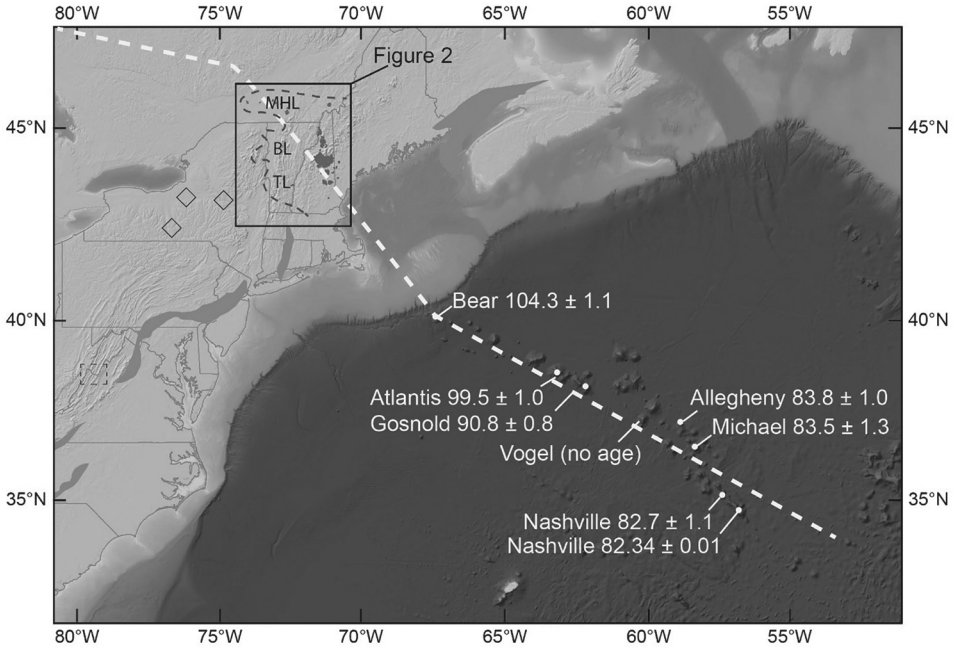

Fig. 1. Location map of the White Mountain Magma Series (WMMS) (plutons in gray), including the western limit of the NEQ (dark dashed line) (McHone, 1984), and New England seamounts. MHL—Monteregian Hills lobe; BL—Burlington lobe; TL—Taconic lobe. $^{40}Ar/^{39}Ar$ ages for the seamounts (white dots) (Duncan, 1984; Merle and others, 2019) are reported in Ma. The white dashed line indicates the Great Meteor hotspot track based on ages of the NEQ and Early Cretaceous WMMS plutons, New England seamounts, and kimberlites in the interior of the continent (Heaman and Kjarsgaard, 2000). Diamonds—New York kimberlites; dashed box—VA/WV postrift magmatism. DEM from NOAA NCEI.

early Mesozoic rifting of Pangea, the eastern North American margin experienced multiple episodes of magmatism including the Jurassic and Early Cretaceous White Mountain Magma Series (WMMS) of northern New England and Quebec (Philpotts, 1970; Foland and Faul, 1977; McHone, 1978; McHone and Butler, 1984; Eby, 1984a, 1984b, 1985a, 1985b, 1985c, 1987; Eby and others, 1992; Roulleau and others, 2012; Roulleau and Stevenson, 2013), Jurassic and Early Cretaceous New York kimberlites (Bailey and Lupulescu, 2015), Jurassic and Eocene intrusions and volcanics of Virginia and West Virginia (Dennison and Johnson, 1971; Mazza and others, 2014, 2017), and the Cretaceous New England seamounts (Duncan, 1984; Merle and others, 2019). Although this postrift magmatism was widespread, particularly in the northern New England portion of the eastern North American margin, the timing and driving mechanisms are generally poorly understood.

The Great Meteor hotspot has persisted as a leading hypothesis for the origin of the Early Cretaceous portion of the WMMS and the Cretaceous New England seamounts (fig. 1) (Morgan, 1972; Sleep, 1990; Heaman and Kjarsgaard, 2000; Rondenay and others, 2000). Morgan (1972) was the first to note an apparent age progression between the Early Cretaceous WMMS and the younger New England seamount chain. Crough (1981) attributed apatite fission track evidence for Early Cretaceous uplift in New England to passage of the hotspot. Duncan (1984) established an age progression for the New England seamounts based on $^{40}Ar/^{39}Ar$ ages for dredged seamount samples. More recently, Heaman and Kjarsgaard (2000) interpreted kimberlites

within the Canadian Shield as belonging to the hotspot track, extending the track northwest to Rankin Inlet on the northwest shore of Hudson Bay.

Other workers have concluded an alternative mechanism is necessary to explain Early Cretaceous WMMS magmatism for the New England and Quebec region. McHone (1978) suggested the Early Cretaceous mafic dikes within New England are associated with long-term tectonically reactivated fractures. Eby (1984a) argued for a similar mechanism of magma generation and noted the span of continental magmatism is inconsistent with a hotspot track. Faure and others (1996) suggested the Early Cretaceous magmatism of Quebec resulted from northward propagation of the Atlantic Ocean under stress conditions that were favorable for local extension and lithospheric thinning. In a review of northeastern North American Mesozoic magmatism, McHone (1996) evaluated and refuted the Great Meteor hotspot hypothesis by arguing that the postrift intrusions are too widespread for a hotspot track and that the published geochronology does not support a consistent age progression. Roulleau and Stevenson (2013) concluded that the Early Cretaceous magmatism of Quebec was linked to rifting and reactivation of structurally weakened lithosphere while Bailey and others (2017) reached a similar conclusion for the Early Cretaceous magmatism of easternmost New York state. Merle and others (2019) concluded that the New England seamount chain, the least-contested portion of the hotspot track, does not display a clear age progression and that a different mechanism is required to explain the magmatism.

Here we present new $^{40}Ar/^{39}Ar$ and U–Pb ages to address the timing of magmatism and evaluate the hotspot model of magmatism for the New England portion of the New England-Quebec igneous province (NEQ), a subdivision of the WMMS. The geochronological evidence presented indicates an extended episode of magmatism that cannot be explained by a hotspot and emphasizes the importance of high accuracy geochronology in assessing potential driving mechanisms for intraplate magmatism. Recognition of postrift magmatism in New England that is not attributable to a hotspot is critical to evaluating the role of processes such as edge-driven convection that may be inherent to passive margin evolution.

GEOLOGIC BACKGROUND

The eastern North American margin is a passive margin established by rifting of Pangea and formation of the Atlantic Ocean. Rifting, which generally occurred along zones of preexisting weakness associated with Mesoproterozoic and Paleozoic collisional orogenesis, began in the Late Triassic (Withjack and others, 2012). Rift-basin sedimentary fill indicates rifting within the New England region continued into the Early Jurassic while rifting to the north continued into the Early Cretaceous (Withjack and others, 2012). Tholeiitic flood basalts of the Central Atlantic Magmatic Province (CAMP) occurred at 201 Ma (Blackburn and others, 2013) and are interbedded with the Jurassic sedimentary deposits of the rift basins. The Hartford–Deerfield and Pomperaug basins, prominent half-graben structures within southern New England, represent the crustal expression of this youngest major tectonic event within New England.

The White Mountain Magma Series (WMMS) is a broadly defined igneous province that includes Mesozoic plutons and sheet intrusions of northern New England and the Montreal region of Quebec (Foland and Faul, 1977). The WMMS includes the Jurassic (200–160 Ma) plutonic complexes and geographically overlapping Early Cretaceous (130–110 Ma) plutons of the White Mountains and Maine (Foland and Faul, 1977; McHone and Butler, 1984; Eby, 1987, Eby and others, 1992) and the postrift NEQ (McHone and Butler, 1984) (fig. 1).

The Early Cretaceous NEQ consists of plutonic complexes and sheet intrusions that are concentrated toward the western limit of the province and distributed into three east–west trending lobes: the Monteregian Hills lobe (north of ~45°N),

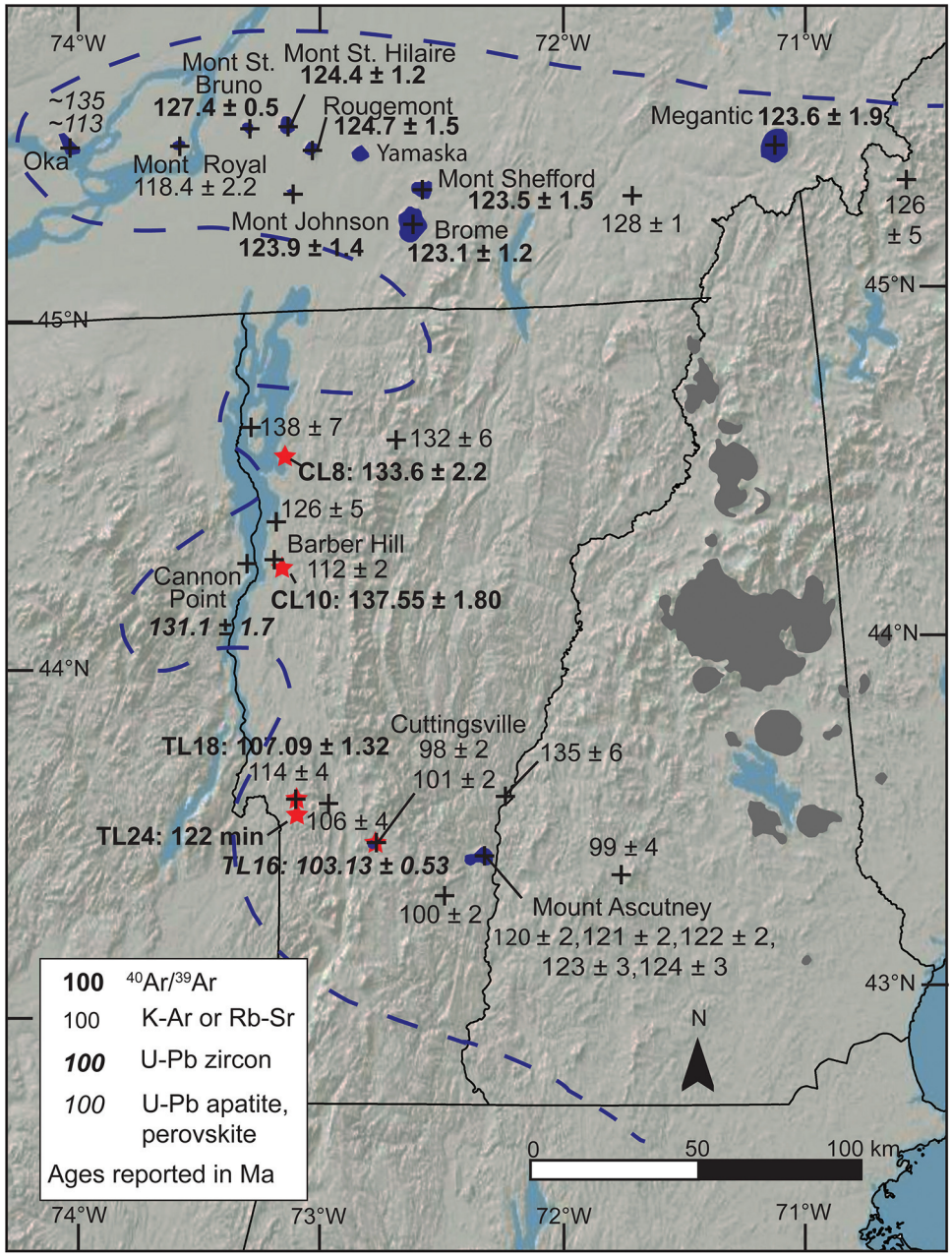

Fig. 2. Map summarizing previously published geochronological data (black crosses) and the results of this investigation (red stars) for NEQ (dashed blue line—province boundary). NEQ plutons (blue) and sheet intrusions are distributed within three lobes (north to south): the Monteregian Hills lobe (45°–46° N), Burlington lobe (44°–45° N), and Taconic lobe (43°–44°N). Dikes not shown. In cases where multiple ages are available for a pluton or sheet intrusion, only the high accuracy ($^{40}Ar/^{39}Ar$ or U–Pb) date is reported. The $^{40}Ar/^{39}Ar$ ages for the Monteregian Hills lobe are the published interpretation of multiple analyses reported by Foland and others (1986) and Gilbert and Foland (1986). All K–Ar ages have been updated using the decay constant of Renne and others (2010) except for the age of the Gassetts dike, the southernmost age reported on the map. The 126 Ma Rb–Sr age in the Burlington lobe (McHone and Corneille, 1980) has been updated using the decay constant of Nebel and others (2011), and the location

Burlington lobe (between ~44°N and ~45°N), and Taconic lobe (between ~43°N and ~44°N) (McHone, 1978) (figs. 1 and 2). The Monteregian Hills lobe of southern Quebec is characterized by a linear belt of ten plutonic complexes (Philpotts, 1970; Eby, 1984a). In contrast, the Burlington and Taconic lobes to the south each contain two small plutonic complexes and are dominated by dikes with a few hundred dikes mapped in the immediate study area of this investigation (McHone, 1978, 1984; Eby, 1985c; Ratcliffe and others, 2011). Many of the dikes are limited in exposure to single outcrops and are typically less than a meter in width while some of the larger dikes are more extensive and wide enough to be traceable for distances up to 5 km. Mafic to intermediate lamprophyres make up the majority of NEQ dikes along with some trachytes (McHone, 1978; Eby, 1985c). The plutons of the Burlington and Taconic lobes are predominantly syenite (Laurent and Pierson, 1973) while the plutons of the Monteregian Hills lobe are more diverse in composition (Eby, 1984b, 1985a).

The plutons and dikes of the NEQ coincide with the Northern Appalachian Anomaly (NAA). The NAA is a shallow mantle low velocity anomaly and the strongest of three anomalies beneath the Appalachians (Shen and Ritzwoller, 2016). Recent high-resolution seismic imaging suggests the NAA is due to modern upwelling beneath the region as a result of edge-driven convection (Menke and others, 2016, 2018; Dong and Menke, 2017; Levin and others, 2018).

Published ages for the New England portion of the NEQ range from 138 Ma to 98 Ma (Appendix tables A1 and A2), but this age range is poorly constrained because it is based mainly on K–Ar and Rb–Sr analyses (Zartman and others, 1967; Armstrong and Stump, 1971; Zen, 1972; Wanless and others, 1973; Foland and Faul, 1977; McHone, 1978, 1984; McHone and Corneille, 1980; Eby, 1984a, 1985c; McEnroe, 1996; Bailey and others, 2017). The K–Ar ages, which in some cases are based on whole-rock analysis or partially altered minerals, are potentially impacted by argon loss or the presence of excess argon. The sole Rb–Sr age has a large uncertainty of ± 5 Ma. The previously published ages reported here have been updated, where data are available, using the decay constants of Renne and others (2010) and Nebel and others (2011). The ages and their sources are listed in Appendix table A1, and recalculated ages, along with originally published ages, are reported in Appendix table A2. The only high accuracy published age for the New England portion of the NEQ is an LA-ICP-MS U–Pb age for a sill at Cannon Point on the New York shore of Lake Champlain (Bailey and others, 2017).

Evaluation of the hotspot model for magmatism in the New England portion of the NEQ is not possible using the previously published data. Prior to publication of the $^{40}Ar/^{39}Ar$ data for the Monteregian Hills lobe, Rb–Sr and fission track ages were interpreted as suggesting magmatism of the Monteregian Hills plutons spanned greater than 30 Ma (Eby, 1984a). This age range is similar to the age range suggested by the K–Ar and Rb–Sr data for the New England portion of the NEQ. In the Monteregian Hills lobe, $^{40}Ar/^{39}Ar$ data, however, have established that the magmatism was a short 1 to 2 Ma duration event around 124 Ma (Foland and others, 1986; Gilbert and Foland, 1986). With limited high accuracy geochronology available for the New England NEQ magmatism, the possibility has remained that all NEQ

Fig. 2. *continued*
is approximate. The original published ages and updated ages are provided in the Appendix tables. WMMS (gray) and NEQ plutons from McHone (1984) and Hibbard and others (2006). NEQ boundary from McHone (1984). Data sources for geochronological data are Zartman and others (1967), Shafiqullah and others (1970), Armstrong and Stump (1971), Zen (1972), Wanless and others (1973), Foland and Faul (1977), McHone (1978, 1984), McHone and Corneille (1980), Eby (1984a, 1985c), Foland and others (1986), Gilbert and Foland (1986), McEnroe (1996), Chen and Simonetti (2014), and Bailey and others (2017). Hillshade map produced from SRTM data.

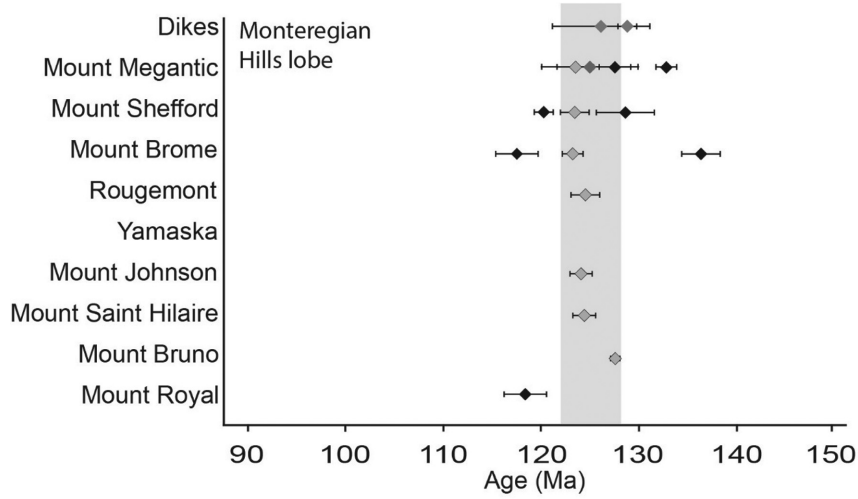

Fig. 3. Summary of age data for plutons and dikes of the Monteregian Hills lobe. Light gray diamonds with black border—$^{40}Ar/^{39}Ar$ ages, black diamonds—Rb–Sr ages, and dark gray diamonds—K–Ar ages. The gray bar represents the interpreted span of magmatism for the Monteregian Hills lobe (Foland and others, 1986). $^{40}Ar/^{39}Ar$ ages from Foland and others (1986) and Gilbert and Foland (1986). Rb–Sr ages from Eby (1984a, 1985c). K–Ar ages from Wanless and others (1973) and McHone (1984). K–Ar ages have been updated using the decay constant of Renne and others (2010) and are reported in Appendix tables A1 and A2.

magmatism occurred as a brief event around 124 Ma. This unanswered question has prevented progress on understanding the timing and origin of NEQ magmatism.

Previous Work on NEQ Pluton Geochronology

The Burlington lobe plutons include the Barber Hill stock in Charlotte, Vermont, and the sills of Cannon Point, New York (fig. 2). Bailey and others (2017) obtained an LA-ICP-MS U–Pb date of 131.1 ± 1.7 Ma for the upper trachyte sill at Cannon Point. A partially chloritized biotite from the Barber Hill stock was dated by K–Ar to 112 ± 2 Ma (Armstrong and Stump, 1971), but this age is suspected to be too young because of alteration and argon loss (McHone and Corneille, 1980). The Barber Hill example illustrates the difficulties associated with relying on the existing K–Ar ages to constrain the timing of magmatism in the New England portion of the NEQ.

The Taconic lobe plutons, the Cuttingsville complex and the Mount Ascutney complex, have both been dated by K–Ar geochronology (fig. 2). No high accuracy geochronology has been published, however, to confirm the pluton ages. Armstrong and Stump (1971) reported two K–Ar ages for the Cuttingsville complex, a biotite age of 98 ± 2 Ma for a biotite syenite unit and a biotite age of 101 ± 2 Ma for essexite. Foland and Faul (1977) reported six K–Ar ages for the different units underlying Mount Ascutney, including granite, syenite, diorite, and gabbro. The ages, which are between 120 ± 2 Ma and 124 ± 3 Ma, suggest a brief period of magma emplacement for the plutonic complex.

Eight of the Monteregian Hills lobe plutonic complexes have been dated by $^{40}Ar/^{39}Ar$ geochronology, and the results have been interpreted to support a short 1 to 2 Ma duration event around 124 Ma (Foland and others, 1986; Gilbert and Foland, 1986) (figs. 2 and 3). The Yamaska and Mount Royal plutons have not been dated using $^{40}Ar/^{39}Ar$ geochronology.

Despite the well-established brief period of magmatism interpreted for the Monteregian Hills plutons, some questions remain regarding the overall timing of magmatism within this region. Recent LA-ICP-MS U–Pb apatite and perovskite ages for the Oka complex, a carbonatite complex just west of the ten silicate plutons of the Monteregian Hills, support magmatism spanning from 135 to 114 Ma (Chen and Simonetti, 2014). The time span of magmatism for the Oka complex is distinct from the brief episode of Monteregian Hills magmatism. The Oka complex timing is also similar to the published Rb–Sr and apatite fission track ages for the Monteregian Hills plutons which are bimodal and cluster around 118 Ma and greater than 130 Ma (Eby, 1984a).

Previous Work on NEQ Dike Geochronology

Seven K–Ar ages and one Rb–Sr age have been published for dikes of the Burlington and Taconic lobes (fig. 2). The two published K–Ar ages that are available for the dikes of the Burlington region include an age of 132 ± 6 Ma for a dike in Cambridge, Vermont (McHone, 1978), and an age of 138 ± 7 Ma for a dike on the western shore of Grand Isle, Vermont (Zartman and others, 1967). Both ages were determined from mineral separates, the Cambridge dike from hornblende and Grand Isle dike from biotite. McHone and Corneille (1980) reported a whole-rock Rb–Sr isochron age of 126 ± 5 Ma based on samples collected from eight trachyte dikes in Shelburne, Vermont, and vicinity. Of the five K–Ar dates that have been published for dikes in the Taconic lobe, the oldest is a whole-rock age of 135 ± 6 Ma for a dike in North Hartland, Vermont (McHone, 1984), while the youngest is a whole-rock age of 99 ± 4 Ma for a dike in Sutton, New Hampshire (McHone, 1978). The published ages for dikes in the western part of the Taconic lobe cluster more closely together and include a whole-rock age of 100 ± 2 Ma for a dike in Gassetts, Vermont (McEnroe, 1996), a hornblende mineral separate age of 106 ± 4 Ma for a dike along U.S. Route 4 in West Rutland, Vermont (Zen, 1972), and a whole-rock age of 114 ± 4 Ma for a dike in Castleton, Vermont (McHone, 1984).

Two published K–Ar ages are available for the dikes of the Monteregian Hills lobe and include an age of 128 ± 1 Ma for a dike in Sherbrooke, Quebec (Wanless and others, 1973), and an age of 126 ± 5 Ma for a dike in western Maine (McHone, 1984) (fig. 2). Fission track data suggest dike emplacement occurred between 139 to 129 Ma, 121 to 117 Ma, and 110 to 107 Ma (Eby, 1985c), and the more recently published ages for the Oka complex (Chen and Simonetti, 2014) support the possibility of an extended period of dike emplacement within the Monteregian Hills region.

METHODOLOGY

The samples targeted for geochronology and the chosen methodology were driven by sample mineralogy. $^{40}Ar/^{39}Ar$ geochronology was selected for the lamprophyre sheet intrusions because of the presence of K-rich mineral phases such as biotite and amphibole, and analysis was completed at the University of Vermont's Noble Gas Geochronology Laboratory. The dikes selected for $^{40}Ar/^{39}Ar$ analysis include representative sheet intrusions from both the Burlington and Taconic lobes. LA-ICP-MS U–Pb dating was selected for the quartz syenite unit of the Cuttingsville complex because of the abundance of zircon within the sample, and the analysis was completed at the University of Arizona's LaserChron Center. The Cuttingsville complex was chosen for U–Pb geochronology to assess the validity of the young K–Ar ages reported in the literature for the complex.

$^{40}Ar/^{39}Ar$ Geochronology

Two lamprophyre dikes from the Burlington lobe and two from the Taconic lobe were selected for $^{40}Ar/^{39}Ar$ geochronology (table 1, fig. 2). A petrographic survey of

TABLE 1

Samples selected for geochronology

Sample ID	Location	NEQ Lobe	Rock Type	Minerals Targeted	Methodology
CL8	44.597336°, -73.196853°	Burlington	Lamprophyre dike	biotite	$^{40}Ar/^{39}Ar$
CL10	44.278183°, -73.218419°	Burlington	Lamprophyre dike	biotite, amphibole	$^{40}Ar/^{39}Ar$
TL18	43.617333°, -73.17687°	Taconic	Lamprophyre dike	amphibole	$^{40}Ar/^{39}Ar$
TL24	43.573906°, -73.178030°	Taconic	Lamprophyre dike	biotite	$^{40}Ar/^{39}Ar$
TL16	43.486800°, -72.881840°	Taconic	Quartz syenite from Cuttingsville complex	zircon	LA-ICP-MS U-Pb

dikes from the study area was completed in order to select the least altered dikes with viable target mineralogy. Samples were collected from the interior of each dike away from the chilled margins and to avoid as much alteration as possible. Mineral separation of biotite and amphibole was completed at the University of Connecticut and the University of Vermont. Visible alteration was removed from each sample, and samples were hand-crushed to the natural grain size of the target minerals. Inclusion-free biotite and amphibole grains were hand-picked using a stereomicroscope. Mineral grains targeted for analysis were washed in an ultrasonic bath and dried to remove any adhering particulate matter. Grains were loaded into aluminum foil packets, arranged in a suprasil vial, and placed in an aluminum canister for irradiation.

Mineral separates from the selected dikes were irradiated at the Oregon State University Radiation Center in the CLOCIT facility for 18 hours with multigrain aliquots of Fish Canyon Tuff sanidine to act as a flux monitor (28.201 ± 0.046 Ma; Kuiper and others, 2008). Laser step heating for $^{40}Ar/^{39}Ar$ dating was conducted with a Santa Cruz Laser Microfurnace 75 W diode laser system. Samples were loaded directly into wells in a copper sample holder. The gas released during heating was purified with SAES getters, and argon isotopes were analyzed on a Nu Instruments Noblesse magnetic sector noble gas mass spectrometer in peak-hopping mode during step-heating analyses. Data from samples and flux monitors were corrected for blanks, mass discrimination, atmospheric argon, neutron-induced interfering isotopes, and the decay of ^{37}Ar and ^{39}Ar. Correction factors used to account for interfering nuclear reactions for the irradiated samples are from Rutte and others (2018), and decay constants are from Min and others (2000) and Stoenner and others (1965). Mass discrimination was calculated by analyzing known aliquots of atmospheric argon for which the measured $^{40}Ar/^{36}Ar$ (294.4 ± 0.26) was compared with an assumed atmospheric value of 298.56 (Lee and others, 2006). A linear interpolation was used to calculate J factors for samples based on sample position between flux monitor packets in the irradiation tube. The data analyses were achieved using both an in-house data reduction program and Isoplot 3.0 (Ludwig, 2003). Plateau ages are reported if sufficient criteria were met (McDougall and Harrison, 1999). Errors on plateaus and weighted mean ages are quoted at the 2σ-level and include precision associated with measurement of the irradiation parameter, J, for flux monitors.

LA-ICP-MS U–Pb Zircon Geochronology

A sample of the quartz syenite of the Cuttingsville complex of the Taconic lobe was selected for LA-ICP-MS U–Pb geochronology (table 1, fig. 2). Zircon extraction was completed at the University of Connecticut using standard mineral separation

methods. The whole-rock sample was hand-crushed, sieved to <450 μm, water panned by hand to remove the lighter minerals from the sample, run through a Frantz magnetic separator, and density-separated using sodium polytungstate (density of 2.85 g/cc). Zircons were hand-selected under ethyl alcohol using a stereomicroscope and mounted in epoxy resin together with fragments of the Sri Lanka standard zircon. The mounts were polished to a depth of ~20 μm, cathodoluminescence (CL) imaged, and cleaned prior to isotopic analysis. The highest-quality grains, including those free of internal fractures, were selected from a CL image, and individual U–Pb ages were successfully determined for 29 of the zircon grains.

U–Pb geochronology was conducted by laser ablation multicollector inductively coupled plasma mass spectrometry (LA-MC-ICPMS) at the University of Arizona LaserChron Center (Gehrels and others, 2008). The analyses involved ablation of zircon with a Photon Machines Analyte G2 Excimer laser using a spot diameter of 30 μm. The ablated material was carried in helium into the plasma source of a Nu HR ICPMS, equipped with a flight tube of sufficient width that U, Th, and Pb isotopes were measured simultaneously. All measurements were made in static mode, using Faraday detectors with $3x10^{11}$ ohm resistors for ^{238}U, ^{232}Th, $^{208}Pb/^{206}Pb$, and discrete dynode ion counters for ^{204}Pb and ^{202}Hg. Ion yields are ~0.8 mv per ppm. Each analysis consisted of one 15-second integration on peaks with the laser off (for backgrounds), 15 one-second integrations with the laser firing, and a 30-second delay to purge the previous sample and prepare for the next analysis. The ablation pit is ~15 μm in depth. Data reductions were completed using the LaserChron Center's program developed by G. Gehrels and the routines of Isoplot (Ludwig, 2003). Individual zircon grain $^{206}Pb/^{238}U$ ages were calculated using the decay constants of Jaffey and others (1971). A weighted mean age was calculated using the 29 individual zircon $^{206}Pb/^{238}U$ grain ages in order to determine an age for the quartz syenite unit.

RESULTS

$^{40}Ar/^{39}Ar$ Geochronology

Burlington lobe dike CL10 from Charlotte, Vermont (fig. 2), is a mafic lamprophyre dike dominated by coarse (~0.5–0.75 mm) augite, amphibole, and some biotite phenocrysts within a finer-grained (~0.1–0.2 mm) biotite and amphibole matrix with some plagioclase, oxides, and calcite. Some of the coarse-grained biotite and amphibole appears altered to chlorite and other fine-grained alteration minerals while the fine-grained biotite and amphibole are unaltered. The fine-grained biotite and amphibole were targeted for analysis. Both amphibole and biotite were dated from CL10 (figs. 4 and 5). A plateau age of 136.9 ± 4.2 Ma with an MSWD of 6.7 and a plateau age based on 87.6 percent of ^{39}Ar was obtained for the amphibole. A plateau age of 137.55 ± 1.80 Ma was calculated for the biotite with an MSWD of 1.4 that included 66.8 percent of ^{39}Ar. Both the amphibole and biotite produced inverse isochron ages consistent with the plateau ages (Appendix tables A3 and A4).

Burlington lobe dike CL8 from Colchester, Vermont (fig. 2), is a mafic lamprophyre dike dominated by biotite and containing some amphibole phenocrysts. Some of the coarse-grained biotite phenocrysts exceed 1 cm in length. The matrix consists of plagioclase, calcite, oxides, and very fine-grained biotite. Calcite is also present within ocelli. Alteration of biotite is minimal. Biotite was dated from CL8 (fig. 6), and a plateau age of 133.6 ± 2.2 Ma was calculated with an MSWD of 2.5 and 73.5 percent of the ^{39}Ar. This sample did not yield an inverse isochron age using all steps. However, an inverse isochron age of 132.5 ± 7.6 Ma was calculated for the steps that yielded the plateau age (Appendix table A5).

Taconic lobe dike TL18 from Castleton, Vermont (fig. 2), is a spessartite lamprophyre dike dominated by alkali feldspar intergrown with augite. Phenocrysts of coarse-

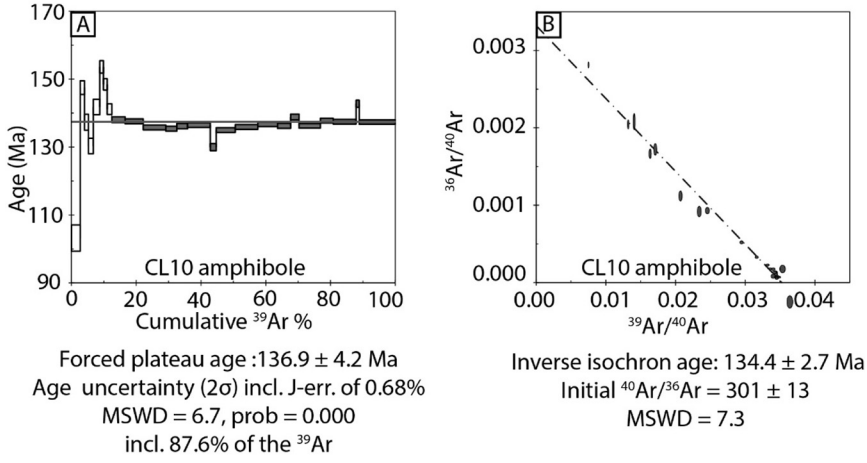

Fig. 4. (A) Apparent age spectra and (B) inverse isochron diagram for Burlington lobe dike mineral separate CL10 amphibole. MSWD—mean square of weighted deviates. Plateau age is calculated using the gray apparent age boxes.

grained amphibole are present. Occasional alteration of the amphibole is present, but most of the grains are unaltered. The groundmass consists of biotite and oxides. Amphibole was dated from TL18 (fig. 7) and produced a plateau age of 107.09 ± 1.32 Ma with an MSWD of 1.3 and 62.5 percent of the ^{39}Ar. This sample yielded an inverse isochron age of 103.5 ± 1.4 Ma (Appendix table A6).

Taconic lobe dike TL24 from Poultney, Vermont (fig. 2), is a spessartite lamprophyre dike dominated by intergrown alkali feldspar and augite with occasional biotite phenocrysts. Alteration of the alkali feldspar is common with some chloritization of the biotite. The groundmass consists of biotite, oxides, and apatite. Biotite was dated from TL24 (fig. 8) and did not yield a plateau age or an inverse isochron age. Argon

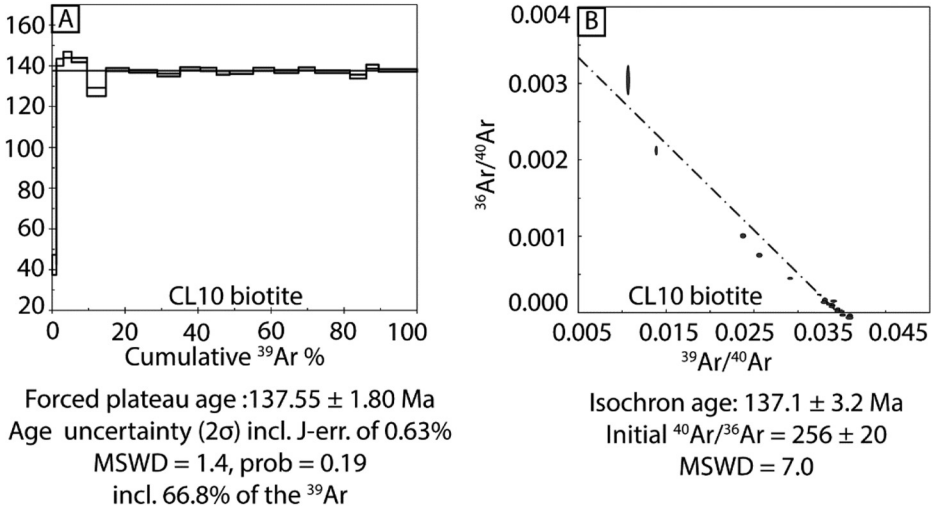

Fig. 5. (A) Apparent age spectra and (B) inverse isochron diagram for Burlington lobe dike mineral separate CL10 biotite. MSWD—mean square of weighted deviates. Plateau age is calculated using the gray apparent age boxes.

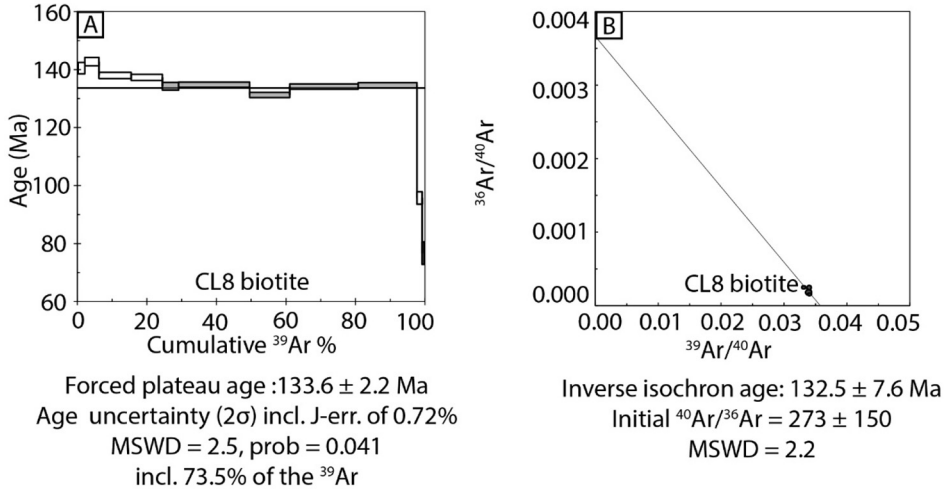

Fig. 6. (A) Apparent age spectra and (B) inverse isochron diagram for Burlington lobe dike mineral separate CL8 biotite. MSWD—mean square of weighted deviates. Plateau age is calculated using the gray apparent age boxes.

released during the lowest-temperature step displays an apparent age of 20 Ma while the oldest apparent age obtained during the higher-temperature stages is 122 Ma (Appendix table A7).

LA-ICP-MS U–Pb Zircon Geochronology

Taconic lobe quartz syenite TL16 from the Cuttingsville complex consists of predominantly alkali feldspar and quartz with some biotite and amphibole. Euhedral pyrite dominates the groundmass. A weighted mean LA-ICP-MS ^{206}Pb/^{238}U zircon age of 103.13 ± 0.53 Ma with an MSWD of 0.64 was determined using the individually

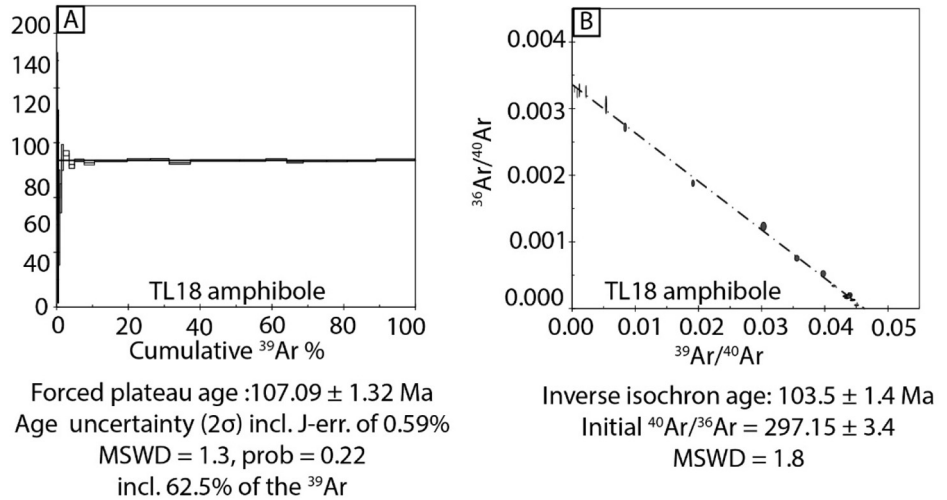

Fig. 7. (A) Apparent age spectra and (B) inverse isochron diagram for Taconic lobe dike mineral separate TL18 amphibole (Castleton dike). MSWD—mean square of weighted deviates. Plateau age is calculated using the gray apparent age boxes.

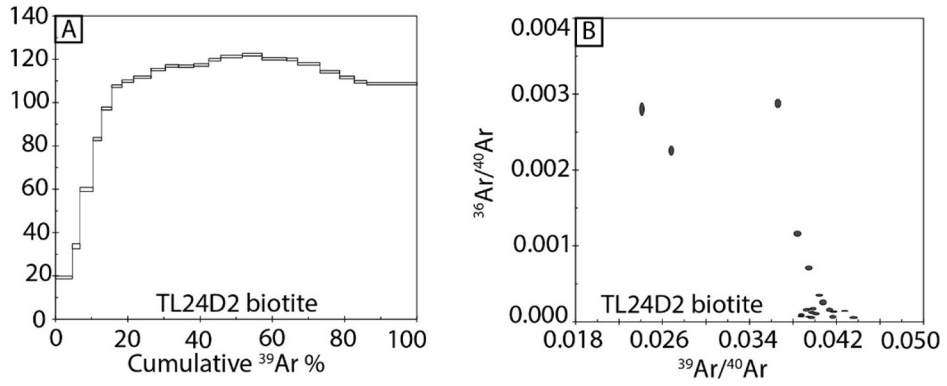

Fig. 8. (A) Apparent age spectra and (B) inverse isochron diagram for Taconic lobe dike mineral separate TL24 biotite (Lewis Brook dike).

dated 29 igneous zircon grains (fig. 9A). The zircon analyses display concordant behavior (fig. 9B) indicating minimal lead loss. The low uncertainty of the weighted mean age is based on the consistent age of the individual zircons dated, ranging from 100.3 ± 1.5 Ma to 105.5 ± 1.5 Ma (Appendix table A8). The zircon crystals display a doubly terminated tetragonal prism form with an elongated c-axis and evidence of zonation. The weighted mean zircon age is interpreted to be a crystallization age for the zircon within the quartz syenite.

DISCUSSION

Timing of Burlington and Taconic Lobe Magmatism

The 137.55 ± 1.80 Ma, 136.9 ± 4.2 Ma, and 133.6 ± 2.2 Ma plateau ages obtained from the dikes of the Burlington lobe are consistent with previously published K–Ar dates for dikes of the region (fig. 10A). Total fusion ages, analogous to K–Ar ages, calculated from the $^{40}Ar/^{39}Ar$ data from this investigation (136.6 ± 0.4 Ma, 136.4 ± 0.4 Ma, and 134 ± 0.8 Ma, respectively) are consistent with the corresponding plateau and inverse isochron ages.

The geochronology for the Burlington lobe from this investigation in combination with the previously published geochronology indicates magmatism within the Burlington lobe spanned about 10 Ma, occurring from approximately 140 Ma to 130 Ma. The U–Pb age of 131.1 ± 1.7 Ma for the upper sill at Cannon Point (Bailey and others, 2017) is the youngest high accuracy age reported for the Burlington lobe. The 112 ± 2 Ma age for the Barber Hill stock (Armstrong and Stump, 1971) represents the only published K–Ar date for the Burlington lobe that suggests magmatism occurred significantly after 130 Ma, and this date is likely the result of argon loss (McHone and Corneille, 1980; Bailey and others, 2017). The lower age limit for Burlington lobe magmatism is interpreted as 129.4 Ma based on the U–Pb age of the Cannon Point sill and lower limit of the analytical uncertainty of the date (fig. 10A). The upper age limit of Burlington lobe magmatism is interpreted as 139.35 Ma based on the $^{40}Ar/^{39}Ar$ biotite age and upper limit of the analytical uncertainty for the dated dike in Charlotte, Vermont (CL10) (fig. 10A). This span of about 10 Ma of magmatism is supported by high accuracy geochronology and is consistent with previously published K–Ar and Rb–Sr geochronology for the Burlington lobe. Younger magmatism within the Burlington lobe has not been identified using $^{40}Ar/^{39}Ar$ or U–Pb geochronology.

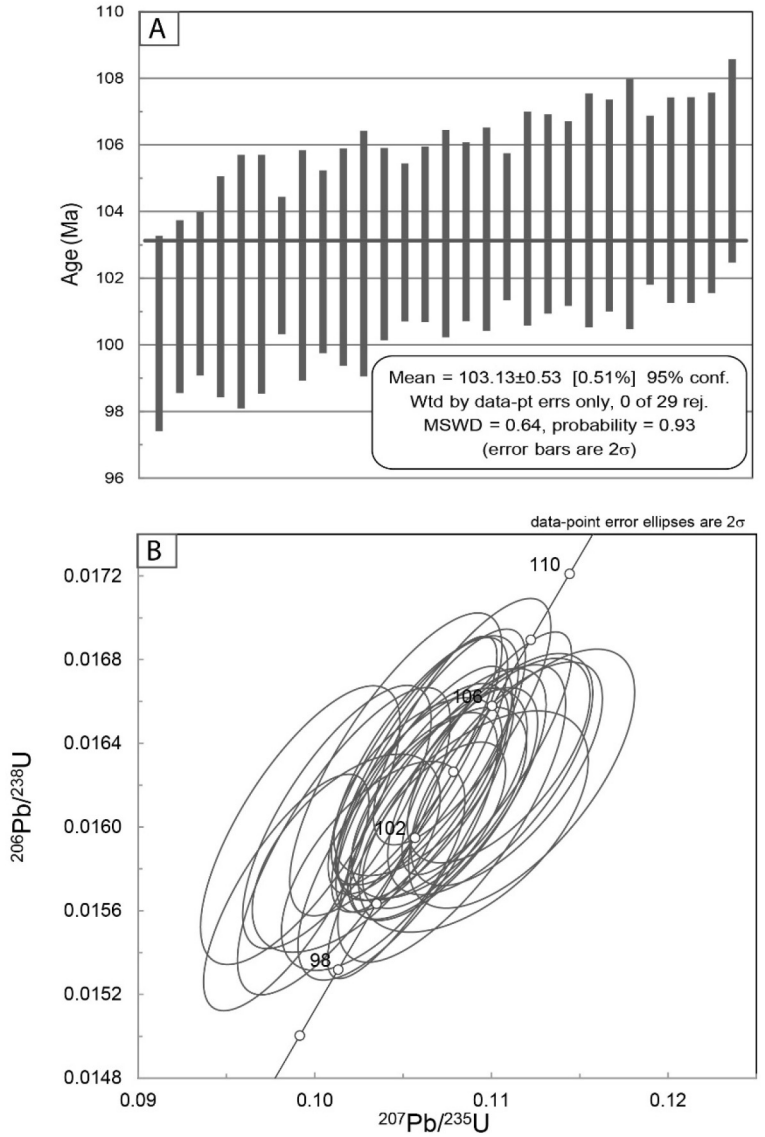

Fig. 9. (A) Weighted mean plot of concordant LA-ICP-MS U–Pb zircon ages for the Cuttingsville quartz syenite (TL16). MSWD—mean square of weighted deviates. (B) Wetherill Concordia diagram of zircon ages used for weighted mean calculation.

The $^{40}Ar/^{39}Ar$ plateau age of 107.09 ± 1.32 Ma for the dike in Castleton, Vermont (TL18), is similar but younger than the whole-rock K–Ar age of 114 ± 4 Ma reported by McHone (1984) for the same dike (fig. 10B). The total fusion age for this dike, calculated from the $^{40}Ar/^{39}Ar$ data from this investigation, is 107.1 ± 0.4 Ma and consistent with the plateau and inverse isochron ages. The dike from Poultney, Vermont (TL24) (Lewis Brook dike in fig. 10B), displays evidence for argon loss and is a minimum of 122 Ma based on the oldest apparent age of the step-heating profile. The weighted mean LA-ICP-MS U–Pb zircon age of 103.13 ± 0.53 Ma for quartz syenite (TL16) from the Cuttingsville complex of the Taconic lobe is consistent with the

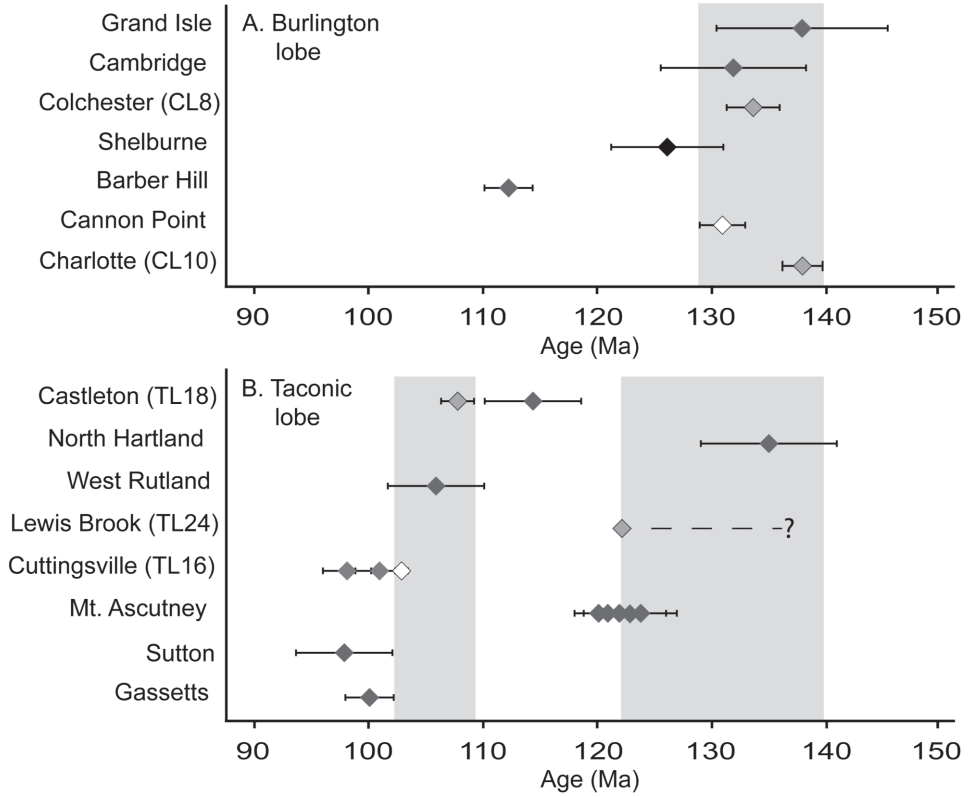

Fig. 10. Summary of age data for plutons and dikes of the (A) Burlington lobe and (B) Taconic lobe. Light gray diamonds with black border—$^{40}Ar/^{39}Ar$ ages, white diamonds with black border—U–Pb ages, black diamond—Rb–Sr age, and dark gray diamonds—K–Ar ages. The gray bars represent the interpreted spans of magmatism. The Colchester (CL8), Charlotte (CL10), $^{40}Ar/^{39}Ar$ Castleton (TL18), Lewis Brook (TL24), and U–Pb Cuttingsville (TL16) ages are from this investigation. Data sources for previously published ages are Zartman and others (1967), Armstrong and Stump (1971), Zen (1972), Foland and Faul (1977), McHone (1978, 1984), McHone and Corneille (1980), McEnroe (1996), and Bailey and others (2017). K–Ar ages (except for the Gassetts dike) have been updated using the decay constant of Renne and others (2010) and are reported in Appendix tables A1 and A2. Rb–Sr age of McHone and Corneille (1980) has been updated using the decay constant of Nebel and others (2011) and is reported in Appendix table A1.

previously published syenite K–Ar age of 101 ± 2 Ma (Armstrong and Stump, 1971). The LA-ICP-MS U–Pb age for the Cuttingsville complex and $^{40}Ar/^{39}Ar$ age for the Castleton dike are also broadly similar to the other previously published K–Ar dates for the western part of the Taconic lobe which cluster around 100 Ma (fig. 10B).

The results of this investigation represent the first $^{40}Ar/^{39}Ar$ and U–Pb geochronology for the Taconic lobe and the first reliable confirmation of an episode of NEQ magmatism younger than the ~124 Ma Monteregian Hills magmatism. The data suggest two episodes of magmatism likely occurred within the Taconic lobe, a younger event that occurred between approximately 110 Ma and 100 Ma and an older event that occurred approximately 122 Ma up to 140 Ma (fig. 10B). The lower age limit of the younger episode of Taconic lobe magmatism is interpreted as 102.6 Ma based on the lower limit of the analytical uncertainty for the U–Pb age for Cuttingsville (TL16) quartz syenite. The lower limit, however, may be younger than documented here because cross-cutting lamprophyre dikes occur within the Cuttingsville quartz syenite

(Ratcliffe and others, 2011). The upper age limit for this younger Taconic lobe magmatism is interpreted as 108.41 Ma based on the upper limit of the analytical uncertainty for the Castleton dike (TL18). The strong argon loss associated with TL24 suggests a minimum age of 122 Ma for the dike, and it is likely that this dike is older and temporally linked to Burlington lobe magmatism. A K–Ar age for the North Hartland dike along the border between Vermont and New Hampshire suggests the dike is 135 ± 6 Ma that is consistent with Burlington lobe magmatism. The lower age limit of this older episode of magmatism could be as young as 122 Ma based on the TL24 minimum age. However, the timing of the older episode of magmatism within the Taconic lobe likely corresponds to the Burlington lobe magmatism since there are no high accuracy ages older than the Castleton dike (TL18) or younger than the Cannon Point sill for the study area. The upper age limit of this older episode of Taconic lobe magmatism is likely similar to the upper age limit of Burlington lobe magmatism at 139 Ma. The Mount Ascutney igneous complex (fig. 2) is likely more closely related to the Early Cretaceous White Mountain plutonic complexes of New Hampshire (Eby, 1987) and represents the only published K–Ar ages for Taconic or Burlington lobe magmatism within the timespan between the younger and older episodes (fig. 10). While the published K–Ar age for the Castleton dike (TL18) falls within this timespan, the $^{40}Ar/^{39}Ar$ data indicate the dike is younger and associated with the younger episode of Taconic lobe magmatism.

The results of this investigation address the longstanding question regarding the span of NEQ magmatism and rule out the possibility of a single short-duration event of magmatism for the entire NEQ. Each lobe of the New England portion of the NEQ represents an episode of magmatism distinct from the ~124 Ma magmatism of the Monteregian Hills lobe (fig. 2) with magmatism occurring between approximately 140 to 130 Ma for the Burlington lobe and a younger episode of Taconic lobe magmatism between approximately 110 to 100 Ma with some older Taconic lobe magmatism likely temporally linked to the Burlington lobe event.

Great Meteor Hotspot Track

The refined timing of Burlington and Taconic lobe magmatism, including the 35 Ma span of magmatism, is based on $^{40}Ar/^{39}Ar$ and U–Pb geochronological data and can be used to assess the validity of the hotspot model and the driving mechanisms behind the magmatism. The following part of the discussion describes the difficulty of fitting the two episodes of magmatism identified in the New England portion of the NEQ to the Great Meteor hotspot track even with adjustments to plate rates. Given the potential for a more complex expression of magmatism through time along a continental hotspot track, in comparison to an oceanic track, this part of the discussion also examines other hypothetical scenarios for hotspot magmatism to explain the timing and location of the Burlington and Taconic lobe magmatism.

The Burlington and Taconic lobe episodes of magmatism do not fit easily with the hotspot track established by Duncan (1984) based on the New England seamount age progression (figs. 1 and 11). Duncan (1984) used the $^{40}Ar/^{39}Ar$ seamount ages to calculate a rate of North American plate motion of 4.7 cm/yr for the Cretaceous. The ~140 to 130 Ma Burlington lobe magmatism is about 20 Ma too old while the ~110 to 100 Ma Taconic lobe magmatism is about 10 Ma too young to fit the hotspot track assuming Duncan's (1984) plate rate of 4.7 cm/yr for the Early Cretaceous (fig. 11).

More recent work has shown that North American absolute plate motion during the Early Cretaceous was likely between 4 to 7 cm/yr and may have slowed to as little as 2.5 cm/yr (Müller and others, 2016). Early Cretaceous plate rates ranging from 2.5 cm/yr to 7 cm/yr do not explain either the Taconic or Burlington lobe magmatism (fig. 11). Both scenarios predict magmatism significantly shorter than the 35 Ma given

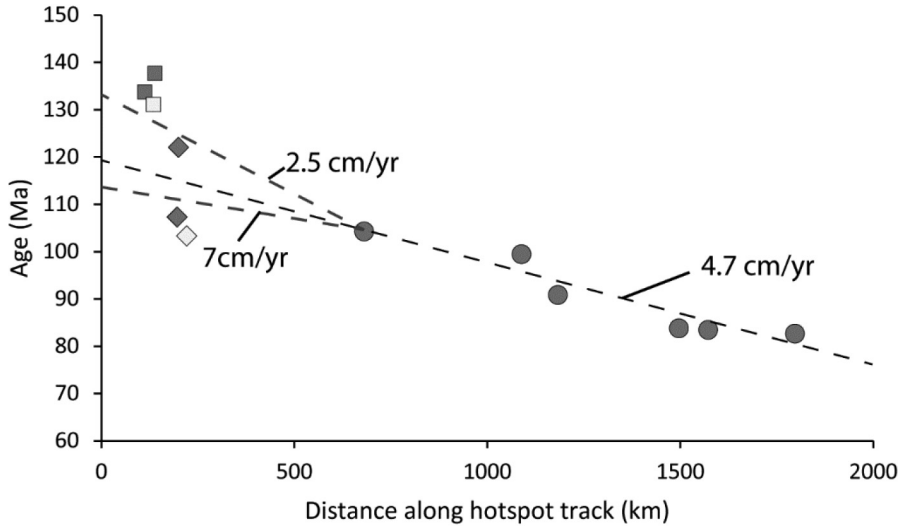

Fig. 11. Graph of age versus distance along Great Meteor hotspot track for intrusions of the Burlington and Taconic lobes and the New England seamounts. Circles—ages for the New England seamounts, squares—ages for the Burlington lobe, diamonds—ages for the Taconic lobe. Gray symbols—$^{40}Ar/^{39}Ar$ ages, white symbols—U–Pb ages, and dashed lines—age versus distance for different plate rates. Modified from Duncan (1984) and McHone (1996).

the magmatism occurs over a distance of approximately 100 km. At the faster plate velocity of 7 cm/yr the magmatism should span only about 1.3 Ma while at the slower plate velocity of 2.5 cm/yr, the magmatism should span only about 4 Ma. The hotspot hypothesis can also be evaluated by considering the predicted hotspot track length that would occur if the magmatism were a product of the hotspot (Eby, 1984a). In this case, if the magmatism were a product of a hotspot, the 35 Ma timespan of magmatism would correspond to hotspot track lengths of approximately 900 km and 2,600 km for plate rates of 2.5 cm/yr and 7 cm/yr, respectively.

Continental hotspot tracks can be more complex than oceanic tracks because of variations in lithospheric thickness (Thompson and Gibson, 1991; Ebinger and Sleep, 1998). However, the observations of this investigation are inconsistent with a complex hotspot expression as a result of varying lithospheric thickness. While plume-related magmatism is known to occur up to 1000 km from the plume source (Thompson and Gibson, 1991; Ebinger and Sleep, 1998), this long-distance transport occurs in locations where asthenospheric flow is aided by a lithospheric gradient from regions of thicker to thinner lithosphere. This possibility for Taconic lobe magmatism can be evaluated by comparing the plume location at the time of Taconic lobe magmatism to the lithospheric structure of the region. The Cuttingsville complex (103.13 ± 0.53 Ma) of southern Vermont and Bear seamount (104.3 ± 1.1 Ma) are 600 km apart and the magmatism in the two locations is nearly contemporaneous with ages differing by no more than ~3 Ma given the analytical uncertainty. A plume location beneath Bear seamount at 104 Ma fits well with plate reconstructions (Duncan, 1984; Sleep, 1990), and Bear seamount is located within thinner lithosphere of the oceanic rise near the ocean-continent transition. If the magmatism of the Cuttingsville complex were also related to the same plume, asthenospheric plume material would need to migrate beneath thicker lithosphere toward the Cuttingsville location. Geophysical evidence supports an increase in lithospheric thickness across the ocean-continent transition into New England (Rychert and others, 2005, 2007), which is the opposite of that

needed to transport plume-related material from Bear seamount to the Cuttingsville region.

Plume head magmatism, which can explain complex patterns of continental hotspot magmatism (Thompson and Gibson, 1991; Ebinger and Sleep, 1998; Jordan and others, 2004), is an unlikely source of Burlington and Taconic lobe magmatism. The 196.2 ± 2.8 Ma Rankin Inlet kimberlites, on the northwest shore of Hudson Bay approximately 3000 km distant from the Burlington and Taconic lobes, are interpreted as the oldest kimberlites attributed to the Great Meteor hotspot track (Heaman and Kjarsgaard, 2000). Plume-head arrival beneath Rankin Inlet is older and likely too far to generate NEQ magmatism according to models of plume-head behavior beneath continental lithosphere. According to these models, plume heads can impact a zone of 500 km in radius (Thompson and Gibson, 1991; Ebinger and Sleep, 1998; Jordan and others, 2004) which is significantly less than the distance between Rankin Inlet and the NEQ.

Recent work by Merle and others (2019) has also cast doubt on the Great Meteor hotspot origin for the New England seamounts. Traditionally, the New England seamounts have been considered the most reliable portion of the Great Meteor hotspot track, yet Merle and others (2019) reassessed the previously published K–Ar and $^{40}Ar/^{39}Ar$ data for the seamounts and concluded that, while an apparent age progression does exist for the seamounts, the age progression is poorly constrained by limited data. They concluded that the New England seamounts are likely genetically linked to other episodes of Late Cretaceous magmatism in the North Atlantic and therefore not the product of a hotspot.

Edge-Driven Convection as a Driving Mechanism

The Burlington and Taconic lobe NEQ magmatism represents one example of postrift passive margin magmatism along the eastern North American margin. Many investigations regarding the timing and origin of these episodes of magmatism report a similar conclusion: the postrift magmatism is not associated with hotspot magmatism and an alternate mechanism is necessary (McHone, 1978, 1996; Mazza and others, 2014, 2017; Bailey and Lupulescu, 2015; Bailey and others, 2017; Merle and others, 2019).

The process of edge-driven convection has been recognized as a potential mechanism to explain passive margin magmatism (King and Anderson, 1995, 1998; King, 2007; Matton and Jebrak, 2009; Kaislaniemi and van Hunen, 2014). This shallow-mantle style of convection can occur beneath regions with a pronounced contrast in lithospheric thickness (King and Anderson, 1995). In a global survey of intraplate magmatism, King (2007) concluded that multiple instances of intraplate magmatism attributed to deep-mantle plumes occur in settings that are conducive to edge-driven convection. Matton and Jebrak (2009) invoked edge-driven convection as one of several factors that may have contributed to Cretaceous magmatism in the Atlantic region. Modern edge-driven convection has been directly linked to Cenozoic magmatism in the Moroccan Atlas Mountains and lithospheric erosion through piecemeal small-scale delamination (Kaislaniemi and van Hunen, 2014).

Edge-driven convection holds the potential to explain Burlington and Taconic lobe magmatism (fig. 12). The magmatism occurs close to the transition between thinner Appalachian and thicker cratonic crust and lithosphere (Li and others, 2018), and the $^{40}Ar/^{39}Ar$ and U–Pb geochronology suggests the magmatism is episodic on the scale of tens of Ma. Geodynamic modeling by Kaislaniemi and van Hunen (2014) shows that magmatism related to edge-driven convection can be episodic on time scales comparable to the timing of Burlington and Taconic lobe magmatism. In

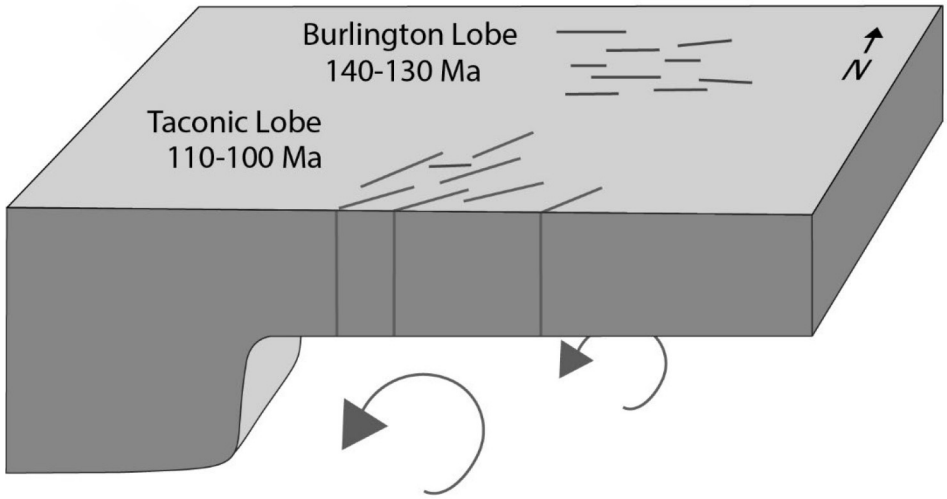

Fig. 12. Schematic diagram illustrating role of edge-driven convection in New England NEQ magmatism.

addition, Amidon and others (2016) have attributed Cretaceous passive margin uplift in New England to the process of edge-driven convection.

Evidence for modern edge-driven convection beneath New England in association with the Northern Appalachian Anomaly (Menke and others, 2016, 2018; Dong and Menke, 2017; Levin and others, 2018) supports the idea that the lithospheric structure beneath the region provides a potential setting for magmatism associated with edge-driven convection. The anomalously thin lithosphere beneath the Appalachians in New England may have resulted from lithospheric erosion through time potentially in association with episodic edge-driven convection (Menke and others, 2018). Levin and others (2018) interpret the modern shallow-mantle upwelling beneath New England as a recent phenomenon. However, the episodic nature of the postrift magmatism investigated here suggests edge-driven convection may have been operating beneath the passive margin of New England since the Early Cretaceous. This early expression of edge-driven convection along the passive margin implies relatively thin lithosphere may have been present as early as the Early Cretaceous in the New England region.

CONCLUSION

The $^{40}Ar/^{39}Ar$ and U–Pb geochronology presented here represents some of the first high accuracy geochronology for the NEQ outside of the Monteregian Hills and confirms an extended period of Early Cretaceous postrift magmatism within New England. Early Cretaceous magmatism in the westernmost part of New England and easternmost New York state within the Burlington and Taconic lobes of the NEQ spans at least 35 Ma. Magmatism of the Burlington lobe occurred at ~140 to 130 Ma while Taconic lobe magmatism occurred at ~110 to 100 Ma. Both episodes of magmatism are distinct from the brief ~124 Ma Monteregian Hills pluton emplacement.

The high accuracy geochronology of this investigation supports the conclusion of McHone (1996) that the magmatism of the New England NEQ is not a product of the Great Meteor hotspot and, therefore, requires an alternate mechanism. Edge-driven convection as a driving mechanism to explain the origin of the New England NEQ is supported by the 35 Ma span of magmatism, its occurrence in proximity to a sharp

contrast in lithospheric thickness, and its episodic nature. This driving mechanism is further supported by the spatial coincidence of the NEQ and NAA. In sum, the results of this investigation emphasize the importance of high accuracy geochronological data in assessing the driving mechanisms behind intraplate and passive margin magmatism.

ACKNOWLEDGMENTS

The geochronological data reported in this investigation was funded by a Geological Society of America student research grant, a Vermont Geological Society student research grant, the Schuele Scholarship provided by the Burlington Gem and Mineral Club, and the University of Connecticut Department of Geosciences. We thank Dan Jones of the University of Vermont for assistance and guidance with the mineral separation and grain selection process for $^{40}Ar/^{39}Ar$ geochronology, Jackie Giblin and Rebecca VanderLeest for assistance with U–Pb analysis, Jessica Robinson and Bryn McGuire for assistance in the field, and Yvette Kuiper and Wallace Bothner for their thoughtful reviews that helped improve this manuscript.

APPENDIX

TABLE A1

Summary of previously published geochronology

NEQ Lobe	Location	Age (Ma)	Method	Source	Comments
MH	Mount Megantic	128 ± 1.7	Rb-Sr	Eby, 1984a	granite whole-rock isochron
MH	Sherbrooke Mine, Quebec lamprophyre	128 ± 1*	K-Ar	Wanless and others, 1973	augite camptonite dike
MH	Dike east of Mt. Megantic,ME	126 ± 5	K-Ar	McHone, 1984	camptonite dike
MH	Mount Megantic	125 ± 5	K-Ar	Eby, 1985c	basaltic dike cutting Mt. Megantic
MH	Mount Megantic	123.6 ± 1.9	$^{40}Ar/^{39}Ar$	Foland and others, 1986	interpreted age based on average total gas age from two biotites in a granite and one in a diorite
MH	Mount Megantic	133 ± 1.1	Rb-Sr	Eby, 1984a	nordmarkite whole-rock isochron
MH	Mount Shefford	123.5 ± 1.5	$^{40}Ar/^{39}Ar$	Foland and others, 1986	interpreted age based on averaged plateau ages for the biotite with amphibole from gabbro
MH	Mount Shefford	129 ± 3	Rb-Sr	Eby, 1984a	pulaskite whole-rock isochron
MH	Mount Shefford	120 ± 1	Rb-Sr	Eby, 1984a	nordmarkite whole-rock isochron
MH	Mount Brome	123.1 ± 1.2	$^{40}Ar/^{39}Ar$	Foland and others, 1986	interpreted age based on average plateau age from amphibole in nepheline diorite and biotite in gabbro
MH	Mount Brome	136 ± 1.7	Rb-Sr	Eby, 1984a	pulaskite whole-rock isochron
MH	Mount Brome	118 ± 2.2	Rb-Sr	Eby, 1984a	nepheline-bearing diorite whole-rock isochron
MH	Rougemont	124.8 ± 1.5	$^{40}Ar/^{39}Ar$	Foland and others, 1986	interpreted age based on average total gas age from biotite in gabbro
MH	Mt. Johnson	123.9 ± 1.4	$^{40}Ar/^{39}Ar$	Foland and others, 1986	interpreted age based on average total gas of biotite from pulaskite
MH	Mt. Bruno	127.4 ± 0.5	$^{40}Ar/^{39}Ar$	Foland and others, 1986	interpreted age for gabbro-pyroxenite average plateau ages considered a maximum age by Foland and others, 1986
MH	Mt. Saint Hilaire	124.4 ± 1.2	$^{40}Ar/^{39}Ar$	Gilbert and Foland, 1986	interpreted age for the complex based on biotite ages
MH	Mount Royal	118 ± 2.2	Rb-Sr	Eby, 1984b	nepheline-bearing diorite whole-rock isochron
MH	Oka complex	~113	U-Pb	Chen and Simonetti, 2014	interpreted age range for younger episode of magmatism at Oka complex based on LA-ICP-MS perovskite and apatite ages
MH	Oka complex	~135	U-Pb	Chen and Simonetti, 2014	interpreted age range for older episode of magmatism at Oka complex based on LA-ICP-MS perovskite and apatite ages
MH	Oka complex	108 ± 6	K-Ar	Shafiqullah and others, 1970	alnoite ring dike
MH	Oka complex	105 ± 5	K-Ar	Shafiqullah and others, 1970	alnoite ring dike
MH	Oka complex	117 ± 7	K-Ar	Shafiqullah and others, 1970	alnoite ring dike
MH	Oka complex	115 ± 6	K-Ar	Shafiqullah and others, 1970	alnoite ring dike
BL	west shore Grand Isle, VT	138 ± 7*	K-Ar	Zartman and others, 1967	lamprophyre dike
BL	Cambridge, VT	132 ± 6*	K-Ar	McHone, 1984	monchiquite lamprophyre dike
BL	Shelburne, VT	126 ± 5*	Rb-Sr	McHone and Corneille, 1980	eight trachyte dikes from South Burlington and Shelburne, VT, whole-rock isochron
BL	Barber Hill stock Charlotte, VT	112 ± 2*	K-Ar	Armstrong and Stump, 1971	biotite age from syenite
BL	Cannon Point sill Essex, NY	131.1 ± 1.7 *	U-Pb	Bailey and others, 2017	LA-ICP-MS zircon age for the upper trachyte sill
TL	Castleton dike Castleton, VT	114 ± 4*	K-Ar	McHone, 1984	spessartite lamprophyre dike
TL	North Hartland, VT	135 ± 6*	K-Ar	McHone, 1978	monchiquite lamprophyre dike
TL	Route 4, West Rutland, VT	106 ± 4*	K-Ar	Zen, 1972	spessartite lamprophyre dike
TL	Cuttingsville complex, VT	101 ± 2*	K-Ar	Armstrong and Stump, 1971	biotite age from essexite
TL	Cuttingsville complex, VT	98 ± 2*	K-Ar	Armstrong and Stump, 1971	biotite age from syenite
TL	Mount Ascutney	122 ± 2*	K-Ar	Foland and Faul, 1977	biotite age from granite
TL	Mount Ascutney	120 ± 2*	K-Ar	Foland and Faul, 1977	biotite age from granite
TL	Mount Ascutney	121 ± 2*	K-Ar	Foland and Faul, 1977	biotite age from granite
TL	Mount Ascutney	122 ± 4*	K-Ar	Foland and Faul, 1977	biotite age from syenite
TL	Mount Ascutney	124 ± 3*	K-Ar	Foland and Faul, 1977	biotite age from diorite
TL	Mount Ascutney	123 ± 3*	K-Ar	Foland and Faul, 1977	biotite age from gabbro
TL	Sutton, NH	99 ± 4*	K-Ar	McHone, 1978	monchiquite lamprophyre dike
TL	Gassetts, VT	100 ± 2	K-Ar	McEnroe, 1996	whole-rock lamprophyre dike age

NEQ lobe: MH–Monteregian Hills lobe, BL–Burlington lobe, and TL–Taconic lobe.
* indicates recalculated age (see Appendix table A2).

TABLE A2

Summary of recalculated K-Ar ages

NEQ Lobe	Location	Updated Age (Ma)	Originally Published Age (Ma)	$^{40}Ar/^{40}K$	Source
MH	Sherbrooke Mine, Quebec	128 ± 1	126 ± 1	0.0788*	Wanless and others, 1973
MH	Dike east of Mount Megantic, ME	126 ± 5	121 ± 5	0.007499	McHone, 1984
BL	Grand Isle, VT	138 ± 7	136 ± 7	0.008414*	Zartman and others, 1967
BL	Cambridge, VT	132 ± 6	130 ± 6	0.00789	McHone, 1978
BL	Barber Hill stock Charlotte, VT	111 ± 2	112 ± 2	0.00667*	Armstrong and Stump, 1971
TL	Castleton dike Castleton, VT	114 ± 4	113 ± 4	0.006794	McHone, 1984
TL	North Hartland, VT	135 ± 6	134 ± 6	0.008081	McHone, 1984
TL	Route 4, West Rutland, VT	106 ± 4	104 ± 4	0.00628*	Zen, 1972
TL	Cuttingville complex, VT	101 ± 2	100 ± 2	0.00599*	Armstrong and Stump, 1971
TL	Cuttingville complex, VT	98 ± 2	96.4 ± 2	0.00578*	Armstrong and Stump, 1971
TL	Mount Ascutney	122 ± 2	120 ± 2	0.00725*	Foland and Faul, 1977
TL	Mount Ascutney	120 ± 2	118 ± 2	0.00712*	Foland and Faul, 1977
TL	Mount Ascutney	121 ± 2	119 ± 2	0.00719*	Foland and Faul, 1977
TL	Mount Ascutney	122 ± 4	120 ± 4	0.00725*	Foland and Faul, 1977
TL	Mount Ascutney	124 ± 3	122 ± 3	0.00737*	Foland and Faul, 1977
TL	Mount Ascutney	123 ± 3	121 ± 3	0.00731*	Foland and Faul, 1977
TL	Sutton, NH	99 ± 4	98 ± 4	0.005882	McHone, 1984

NEQ lobe: MH–Monteregian Hills lobe, BL–Burlington lobe, and TL–Taconic lobe.
* indicates backcalculated $^{40}Ar/^{40}K$. Ratio was calculated from reported age and decay constants.

TABLE A3

$^{40}Ar/^{39}Ar$ analytical data CL10 amphibole

$^{39}Ar/^{40}Ar$	$^{39}Ar/^{40}Ar$ abs error	$^{36}Ar/^{40}Ar$	$^{36}Ar/^{40}Ar$ abs error	cumul. % 39	age (Ma)	1σ%error (noJ)	1σ%error (tot)
0.007519468	4.51097E-05	0.002815895	2.58418E-05	2.666	103.50	3.745	7.71
0.016376787	0.00011195	0.001667979	4.06786E-05	4.036	147.79	1.356	2.58
0.017108737	0.000143948	0.001724057	4.99857E-05	5.252	137.57	1.722	2.83
0.014080696	9.31101E-05	0.002083312	6.99082E-05	6.713	130.59	1.736	3.35
0.013228889	8.26846E-05	0.002047579	3.83543E-05	8.744	142.07	1.600	3.22
0.020735232	0.000162803	0.001121611	4.3116E-05	9.868	153.89	1.179	2.07
0.02342251	0.000191957	0.000920668	4.49723E-05	11.016	148.74	1.128	1.94
0.024590988	0.000197396	0.000932691	2.72455E-05	12.450	141.43	1.110	1.94
0.029495381	0.000155223	0.000523135	1.32429E-05	16.550	138.34	0.621	1.55
0.031665169	0.000155015	0.000330776	1.04007E-05	22.133	137.85	0.540	1.45
0.03323438	0.000157283	0.000229992	8.00552E-06	29.125	136.04	0.505	1.41
0.03437956	0.000175573	0.000132648	1.4363E-05	32.554	135.67	0.528	1.39
0.034821956	0.000198015	7.24767E-05	8.07274E-06	35.852	136.44	0.577	1.39
0.03360228	0.000164329	0.000182396	7.2177E-06	42.841	136.74	0.513	1.39
0.03538324	0.000264404	0.000178572	3.28238E-05	44.704	130.25	0.783	1.51
0.034055293	0.000167689	0.00017574	1.15144E-05	50.553	135.28	0.516	1.39
0.034323849	0.000172557	0.000128809	9.53357E-06	57.529	136.19	0.519	1.38
0.034591775	0.000160401	8.53901E-05	7.86227E-06	63.603	136.93	0.472	1.35
0.034206528	0.000184093	0.000131613	1.21086E-05	67.641	136.55	0.556	1.40
0.034037335	0.000205986	8.49906E-05	1.81391E-05	70.275	139.11	0.616	1.41
0.03444987	0.000163485	0.000109948	9.31869E-06	76.868	136.52	0.487	1.37
0.034542239	0.000169773	6.30772E-05	1.22929E-05	80.813	138.06	0.497	1.36
0.034547166	0.000170519	7.04687E-05	7.0768E-06	87.889	137.74	0.500	1.36
0.036428323	0.000283953	-0.000247132	-5.30813E-05	88.840	143.03	0.720	1.37
0.034467104	0.000156843	7.88493E-05	4.4136E-06	100.000	137.64	0.462	1.35

TABLE A4

$^{40}Ar/^{39}Ar$ analytical data CL10 biotite

$^{39}Ar/^{40}Ar$	$^{39}Ar/^{40}Ar$ abs error	$^{36}Ar/^{40}Ar$	$^{36}Ar/^{40}Ar$ abs error	cumul. % 39	age (Ma)	1σ%error (noJ)	1σ%error (tot)
0.010676533	0.000114288	0.003045098	0.000128119	1.16422	42.49	11.664	16.66
0.023756164	0.000198374	0.001009016	1.925E-05	3.11748	141.85	1.192	2.01
0.025607742	0.000204715	0.000754878	1.72739E-05	5.32371	145.57	1.030	1.80
0.029116059	0.000188341	0.000451879	9.57553E-06	9.60231	142.98	0.747	1.55
0.013882861	8.33517E-05	0.002124018	3.84021E-05	14.7512	127.33	1.639	3.40
0.033069042	0.00018149	0.000166929	1.91384E-05	21.0661	138.27	0.578	1.40
0.034546059	0.000176559	4.5172E-05	1.40902E-05	28.8102	137.44	0.518	1.34
0.035918267	0.000206932	-3.93615E-05	-1.75272E-05	35.0832	135.64	0.569	1.34
0.033855296	0.000203126	8.13892E-05	1.02484E-05	40.5786	138.66	0.615	1.39
0.034530972	0.000214118	2.35679E-05	1.23981E-05	45.0046	138.36	0.624	1.38
0.035868293	0.000257919	-6.10338E-05	-1.56723E-05	48.6419	136.66	0.706	1.39
0.034968179	0.000200594	1.9927E-05	9.39735E-06	55.1171	136.91	0.577	1.36
0.035091494	0.000214641	-2.76374E-05	-9.73646E-06	60.8447	138.37	0.606	1.36
0.033819284	0.00018602	0.000116981	6.65928E-06	67.5279	137.36	0.570	1.38
0.033516922	0.000198973	0.000116334	9.77542E-06	72.0362	138.59	0.615	1.40
0.034004968	0.000163336	0.000100826	4.78274E-06	81.5786	137.29	0.495	1.35
0.03406404	0.00022599	0.000154897	9.50058E-06	86.0635	134.86	0.696	1.45
0.032969424	0.000217459	0.000141182	1.26513E-05	89.447	139.74	0.689	1.44
0.032414645	0.00015072	0.000240239	5.04487E-06	100	137.83	0.501	1.39

TABLE A5

$^{40}Ar/^{39}Ar$ analytical data CL8 biotite

$^{39}Ar/^{40}Ar$	$^{39}Ar/^{40}Ar$ abs error	$^{36}Ar/^{40}Ar$	$^{36}Ar/^{40}Ar$ abs error	cumul. % 39	age (Ma)	1σ%error (noJ)	1σ%error (tot)
0.03194638	0.00041634	0.000224136	0.00012751	1.925	140.31	1.40	1.90
0.033666499	0.00034667	9.3911E-07	5.06876E-05	6.031	142.56	1.03	1.62
0.033744003	0.00025471	0.000108883	2.84434E-05	15.310	137.83	0.78	1.51
0.033912651	0.0002534	0.000109925	2.93251E-05	24.354	137.13	0.77	1.51
0.03394636	0.00031967	0.000181423	2.63208E-05	29.054	134.09	1.00	1.64
0.034081566	0.0002097	0.000155048	1.15371E-05	49.580	134.64	0.65	1.46
0.034019933	0.00022123	0.000247794	1.93675E-05	61.131	131.10	0.70	1.51
0.03316678	0.00020435	0.000256137	1.10743E-05	80.924	134.01	0.67	1.50
0.033141329	0.00020703	0.000248418	1.39633E-05	97.886	134.43	0.67	1.50
0.037084287	0.00060606	0.000907626	0.000133886	99.406	95.69	2.24	2.73
0.033935281	0.00091068	0.0015676	0.000324547	100.000	76.71	5.04	5.39

TABLE A6

$^{40}Ar/^{39}Ar$ analytical data TL18 amphibole

$^{39}Ar/^{40}Ar$	$^{39}Ar/^{40}Ar$ abs error	$^{36}Ar/^{40}Ar$	$^{36}Ar/^{40}Ar$ abs error	cumul. % 39	age (Ma)	1σ%error (noJ)	1σ%error (tot)
0.000383448	7.18725E-06	0.003297578	3.58451E-05	0.160	203.50	114.61	126.22
0.000805525	1.54057E-05	0.003223301	3.95618E-05	0.367	241.08	47.48	51.50
0.001154904	1.60013E-05	0.003273253	6.35275E-05	0.508	124.96	48.85	60.62
0.001189728	1.99563E-05	0.003299934	4.82848E-05	0.738	73.64	95.84	112.80
0.002214936	3.45671E-05	0.003257201	6.17509E-05	1.067	65.50	53.18	64.21
0.005404171	6.32639E-05	0.003059397	8.86707E-05	1.578	79.52	13.35	18.05
0.008416544	0.000138857	0.002721878	4.29055E-05	2.096	109.42	8.71	10.22
0.019164482	0.000140005	0.001882079	3.26472E-05	3.713	112.49	1.65	2.97
0.030339472	0.000285226	0.001235552	4.22528E-05	5.184	102.86	1.47	2.29
0.035616497	0.000248534	0.000758128	2.91383E-05	7.895	107.24	0.89	1.73
0.039780006	0.000262508	0.000527731	2.99218E-05	10.750	104.68	0.77	1.58
0.041461481	0.000196691	0.000344925	1.01145E-05	19.870	106.79	0.52	1.42
0.04324126	0.000228713	0.000185138	7.49292E-06	26.385	107.85	0.55	1.38
0.043518372	0.000224605	0.000163228	9.40541E-06	31.596	107.93	0.54	1.36
0.043997415	0.000226601	0.000219331	1.50259E-05	37.501	105.07	0.54	1.38
0.043768443	0.00022052	0.000170049	7.50339E-06	51.193	107.17	0.52	1.36
0.044370003	0.00021864	0.000128292	6.51351E-06	58.530	107.18	0.51	1.34
0.045064993	0.00021731	5.43824E-05	8.32802E-06	64.346	107.94	0.48	1.31
0.043993936	0.000235807	0.000196615	1.82105E-05	68.977	105.93	0.56	1.38
0.044516212	0.000223929	0.000133619	7.73882E-06	75.458	106.76	0.52	1.35
0.043837763	0.000215053	0.000184417	1.64365E-05	81.245	106.70	0.51	1.36
0.044441974	0.000193038	0.000134267	6.79209E-06	89.259	106.92	0.45	1.32
0.043269519	0.000201332	0.000196093	5.39758E-06	100.000	107.82	0.49	1.35

TABLE A7

$^{40}Ar/^{39}Ar$ analytical data TL24 biotite

$^{39}Ar/^{40}Ar$	$^{39}Ar/^{40}Ar$ abs error	$^{36}Ar/^{40}Ar$	$^{36}Ar/^{40}Ar$ abs error	cumul. % 39	age (Ma)	1σ%error (noJ)	1σ%error (tot)
0.036602932	0.00017582	0.002881441	3.69302E-05	4.632	19.32	3.38	8.52
0.024105333	0.000133482	0.002805445	5.57567E-05	6.785	33.75	3.38	7.54
0.026806294	0.000140166	0.002259361	4.04204E-05	10.384	60.02	1.60	3.75
0.038398951	0.000218569	0.001164297	2.28786E-05	12.757	83.27	0.87	1.95
0.039451545	0.000208187	0.000712891	1.75316E-05	15.564	97.35	0.67	1.62
0.040412366	0.000207554	0.00035289	8.29502E-06	18.370	107.66	0.57	1.43
0.040757158	0.000203029	0.000258523	2.24926E-05	21.629	110.02	0.54	1.39
0.041355314	0.000196058	0.00016	1.51775E-05	26.445	111.81	0.50	1.34
0.039844946	0.000187394	0.000174746	1.12665E-05	30.401	115.37	0.50	1.35
0.039344326	0.000191381	0.000168293	7.82613E-06	34.072	117.03	0.51	1.35
0.040123622	0.000192041	0.000108808	1.10697E-05	38.259	116.91	0.49	1.33
0.03971472	0.000189246	0.00012672	9.96136E-06	42.420	117.45	0.50	1.33
0.039700068	0.000196201	5.90769E-05	7.67259E-06	45.713	119.87	0.50	1.31
0.038762184	0.000177291	9.67016E-05	7.46064E-06	51.718	121.35	0.47	1.31
0.038732894	0.000188365	7.45972E-05	4.75826E-06	57.146	122.23	0.50	1.32
0.039426472	0.000179636	7.05481E-05	4.04644E-06	63.946	120.32	0.47	1.30
0.039684747	0.000204886	5.91408E-05	8.66628E-06	66.996	120.05	0.52	1.32
0.039207253	0.000184899	0.000159331	1.10246E-05	73.189	117.97	0.49	1.34
0.041659281	0.000191887	6.77406E-05	1.2387E-05	78.637	114.31	0.47	1.31
0.041735142	0.000204042	0.00013646	7.16514E-06	82.688	111.72	0.51	1.34
0.043570502	0.000235064	5.84605E-05	8.4759E-06	86.112	109.70	0.55	1.33
0.042753774	0.000192456	0.000144891	4.34344E-06	100.000	108.79	0.47	1.33

TABLE A8

U-Pb zircon analyses for the Cuttingsville quartz syenite (TL16)

Spot	U (ppm)	$^{206}Pb/^{204}Pb$	U/Th	$^{206}Pb^*/^{207}Pb^*$	± (%)	$^{207}Pb^*/^{235}U^*$	± (%)	$^{206}Pb^*/^{238}U$	± (%)	error corr.	$^{206}Pb^*/^{238}U^*$	± (Ma)	$^{207}Pb^*/^{235}U$	± (Ma)	$^{206}Pb^*/^{207}Pb^*$	± (Ma)	Best age (Ma)	± (Ma)
2	224	5805	1.8	21.9729	1.3	0.0984	1.9	0.0157	1.5	0.76	100.3	1.5	95.3	1.8	NA	NA	100.3	1.5
11	214	27475	1.7	21.0961	1.6	0.1033	2.1	0.0158	1.3	0.63	101.1	1.3	99.8	2.0	68.5	38.0	101.1	1.3
22	206	17501	2.1	21.4953	1.8	0.1018	2.1	0.0159	1.2	0.57	101.5	1.2	98.4	2.0	23.7	42.1	101.5	1.2
25	360	36002	1.9	20.9396	1.5	0.1047	2.2	0.0159	1.6	0.75	101.7	1.7	101.1	2.1	86.2	34.8	101.7	1.7
13	248	9715	1.8	21.6006	1.5	0.1017	2.4	0.0159	1.9	0.78	101.9	1.9	98.3	2.3	11.9	36.6	101.9	1.9
26	911	47356	2.6	20.7610	1.0	0.1060	2.0	0.0160	1.8	0.87	102.1	1.8	102.3	2.0	106.4	23.6	102.1	1.8
15	236	47968	1.4	20.6660	1.2	0.1068	1.5	0.0160	1.0	0.65	102.4	1.0	103.0	1.5	117.3	27.6	102.4	1.0
8	186	4347	1.9	22.2446	1.6	0.0992	2.3	0.0160	1.7	0.73	102.4	1.7	96.0	2.1	NA	NA	102.4	1.7
14	145	37479	1.8	20.2664	2.0	0.1090	2.4	0.0160	1.3	0.55	102.5	1.4	105.0	2.4	163.1	47.4	102.5	1.4
17	244	4781	2.5	21.8421	1.4	0.1013	2.2	0.0160	1.6	0.74	102.6	1.6	97.9	2.0	NA	NA	102.6	1.6
19	182	55262	1.9	20.5460	1.6	0.1078	2.4	0.0161	1.8	0.74	102.7	1.8	103.9	2.4	131.0	38.7	102.7	1.8
27	315	21475	1.6	20.6880	1.4	0.1073	2.0	0.0161	1.4	0.70	103.0	1.4	103.5	2.0	114.8	34.0	103.0	1.4
28	192	17580	1.8	20.7525	1.5	0.1070	1.9	0.0161	1.2	0.61	103.1	1.2	103.3	1.9	107.5	35.4	103.1	1.2
16	192	63850	1.5	20.8816	1.6	0.1066	2.1	0.0162	1.3	0.62	103.3	1.3	102.9	2.0	92.7	38.3	103.3	1.3
4	224	16460	2.1	20.7212	1.5	0.1075	2.1	0.0162	1.5	0.71	103.3	1.6	103.7	2.1	111.0	35.6	103.3	1.6
1	175	13746	2.4	20.9917	1.3	0.1062	1.9	0.0162	1.3	0.71	103.4	1.3	102.4	1.8	80.3	31.2	103.4	1.3
23	330	77882	1.7	21.0007	1.2	0.1062	1.9	0.0162	1.5	0.77	103.5	1.5	102.5	1.9	79.2	28.8	103.5	1.5
9	168	14430	1.5	21.0854	1.5	0.1058	1.8	0.0162	1.1	0.58	103.6	1.1	102.2	1.8	69.7	35.4	103.6	1.1
29	252	14000	1.5	20.0241	1.7	0.1117	2.3	0.0162	1.6	0.67	103.8	1.6	107.5	2.4	191.2	40.6	103.8	1.6
24	223	7318	1.6	20.3752	1.6	0.1099	2.2	0.0163	1.4	0.67	103.9	1.5	105.9	2.2	150.6	37.4	103.9	1.5
6	328	64671	1.8	20.2061	1.5	0.1109	2.0	0.0163	1.3	0.67	103.9	1.4	106.8	2.0	170.1	34.5	103.9	1.4
7	407	44080	1.7	21.0659	1.2	0.1064	2.1	0.0163	1.7	0.81	104.0	1.8	102.7	2.1	71.9	29.6	104.0	1.8
5	299	20300	1.7	21.2148	1.2	0.1058	2.0	0.0163	1.5	0.78	104.2	1.6	102.2	1.9	55.1	29.0	104.2	1.6
20	265	9344	1.9	21.4775	1.5	0.1046	2.3	0.0163	1.8	0.77	104.2	1.9	101.0	2.3	25.7	35.7	104.2	1.9
3	239	32353	1.8	20.3683	1.5	0.1104	1.9	0.0163	1.2	0.64	104.3	1.3	106.3	1.9	151.4	34.4	104.3	1.3
18	388	37966	1.8	21.2683	1.0	0.1057	1.8	0.0163	1.5	0.84	104.3	1.5	102.1	1.7	49.1	22.8	104.3	1.5
10	421	12497	2.0	21.1701	1.4	0.1062	2.0	0.0163	1.5	0.73	104.3	1.5	102.5	2.0	60.2	33.0	104.3	1.5
12	410	68308	2.0	20.5376	1.0	0.1097	1.8	0.0164	1.4	0.81	104.6	1.5	105.7	1.8	132.0	24.6	104.6	1.5
21	215	21790	1.6	20.9929	1.2	0.1083	1.9	0.0165	1.5	0.77	105.5	1.5	104.5	1.9	80.1	28.6	105.5	1.5

REFERENCES

Amidon, W. H., Roden-Tice, M., Anderson, A. J., McKeon, R. E., and Shuster, D. L., 2016, Late Cretaceous unroofing of the White Mountains, New Hampshire, USA: An episode of passive margin rejuvenation?: Geology, v. 44, n. 6, p. 415–418, https://doi.org/10.1130/G37429.1

Armstrong, R. L., and Stump, E., 1971, Additional K–Ar dates, White Mountain Magma Series, New England: American Journal of Science, v. 270, n. 5, p. 331–333, https://doi.org/10.2475/ajs.270.5.331

Bailey, D. G., and Lupulescu, M. V., 2015, Spatial, temporal, mineralogical, and compositional variations in Mesozoic kimberlitic magmatism in New York State: Lithos, v. 212–215, p. 298–310, http://dx.doi.org/10.1016/j.lithos.2014.11.022

Bailey, D. G., Lupulescu, M., Chiarenzelli, J., and Taylor, J. P., 2017, Age and origin of the Cannon Point syenite, Essex County, New York: Southernmost expression of the Monteregian Hills magmatism?: Canadian Journal of Earth Sciences, v. 54, n. 4, p. 379–392, https://doi.org/10.1139/cjes-2016-0144

Blackburn, T. J., Olsen, P. E., Bowring, S. A., McLean, N. M., Kent, D. V., Puffer, J., McHone, G., Rasbury, E. T., and Et-Touhami, M., 2013, Zircon U–Pb geochronology links the end-Triassic extinction with the central Atlantic magmatic province: Science, v. 384, n. 6135, p. 941–945, https://doi.org/10.1126/science.1234204

Chen, W., and Simonetti, A., 2014, Evidence for the multi-stage petrogenetic history of the Oka carbonatite complex (Québec, Canada) as recorded by perovskite and apatite: Minerals, v. 4, n. 2, p. 437–476, https://doi.org/10.3390/min4020437

Crough, S. T., 1981, Mesozoic hotspot epeirogeny in eastern North America: Geology, v. 9, n. 1, p. 2–6, https://doi.org/10.1130/0091-7613(1981)9<2:MHEIEN>2.0.CO;2

Dennison, J. M., and Johnson Jr., R. W., 1971, Tertiary intrusions and associated phenomena near the thirty-eighth parallel fracture zone in Virginia and West Virginia: GSA Bulletin, v. 82, n. 2, p. 501–508, https://doi.org/10.1130/0016-7606(1971)82[501:TIAAPN]2.0.CO;2

Dong, M. T., and Menke, W. H., 2017, Seismic high attenuation region observed beneath southern New England from teleseismic body wave spectra: Evidence for high asthenospheric temperature without melt: Geophysical Research Letters, v. 44, n. 21, p. 10,958–10,969, https://doi.org/10.1002/2017GL074953

Duncan, R. A., 1984, Age progressive volcanism of the New England seamounts and the opening of the central Atlantic Ocean: Journal of Geophysical Research-Solid Earth, v. 89, n. B 12, p. 9980–9990, https://doi.org/10.1029/JB089iB12p09980

Ebinger, C. J., and Sleep, N. H., 1998, Cenozoic magmatism throughout east Africa resulting from impact of a single plume: Nature, v. 395, p. 788–791, https://doi.org/10.1038/27417

Eby, G. N., 1984a, Geochronology of the Monteregian Hills alkaline igneous province, Quebec: Geology, v. 12, n. 8, p. 468–470, https://doi.org/10.1130/0091-7613(1984)12<468:GOTMHA>2.0.CO;2

——— 1984b, Monteregian Hills I. Petrography, major and trace element geochemistry, and strontium isotopic chemistry of the western intrusions: Mounts Royal, St. Bruno, and Johnson: Journal of Petrology, v. 25, n. 2, p. 421–452, https://doi.org/10.1093/petrology/25.2.421

——— 1985a, Monteregian Hills II. Petrography, major and trace element geochemistry, and strontium isotopic chemistry of the eastern intrusions: Mounts Shefford, Brome, and Megantic: Journal of Petrology, v. 26, n. 2, p. 418–448, https://doi.org/10.1093/petrology/26.2.418

——— 1985b, Sr and Pb isotopes, U and Th chemistry of alkaline Monteregian and White Mountain igneous provinces, eastern North America: Geochimica et Cosmochimica Acta, v. 49, n. 5, p. 1143–1153, https://doi.org/10.1016/0016-7037(85)90005-5

——— 1985c, Age relations, chemistry, and petrogenesis of mafic alkaline dikes from the Monteregian Hills and younger White Mountains igneous provinces: Canadian Journal of Earth Sciences, v. 22, n. 8, p. 1103–1111, https://doi.org/10.1139/e85-112

——— 1987, The Monteregian Hills and White Mountain alkaline igneous provinces, eastern North America: Geological Society, London, Special Publications, v. 30, p. 433–447, https://doi.org/10.1144/GSL.SP.1987.030.01.21

Eby, G. N., Krueger, H. W., and Creasy, J. W., 1992, Geology, geochronology, and geochemistry of the White Mountain batholith, New Hampshire, *in* Puffer, J. H., and Ragland, P.C., editors, Eastern North American Mesozoic Magmatism: Geological Society of America Special Paper 268, https://doi.org/10.1130/SPE268-p379

Faure, S., Tremblay, A., and Angelier, J., 1996, State of intraplate stress and tectonism of northeastern America since Cretaceous times, with particular emphasis on the New England-Quebec igneous province: Tectonophysics, v. 255, n. 1–2, p. 111–134, https://doi.org/10.1016/0040-1951(95)00113-1

Foland, K. A., and Faul, H., 1977, Ages of the White Mountain intrusives – New Hampshire, Vermont, and Maine, USA: American Journal of Science, v. 277, n. 7, p. 888–904, https://doi.org/doi:10.2475/ajs.277.7.888

Foland, K. A., Gilbert, L. A., Sebring, C. A., and Jiang-Feng, C., 1986, $^{40}Ar/^{39}Ar$ ages for plutons of the Monteregian Hills, Quebec: Evidence for a single episode of Cretaceous magmatism: GSA Bulletin, v. 97, n. 8, p. 966–974, https://doi.org/10.1130/0016-7606(1986)97<966:AAFPOT>2.0.CO;2

Gehrels, G. E., Valencia, V. A., and Ruiz, J., 2008, Enhanced precision, accuracy, efficiency, and spatial resolution of U–Pb ages by laser ablation-multicollector-inductively coupled plasma-mass spectrometry: Geochemistry, Geophysics, Geosystems, v. 9, n. 3, https://doi.org/10.1029/2007GC001805

Gilbert, L. A., and Foland, K. A., 1986, The Mont Saint Hilaire plutonic complex: Occurrence of excess ^{40}Ar and short intrusion history: Canadian Journal of Earth Sciences, v. 23, n. 7, p. 948–958, https://doi.org/10.1139/e86-096

Heaman, L. M., and Kjarsgaard, B. A., 2000, Timing of eastern North American kimberlite magmatism: Continental extension of the Great Meteor hotspot track?: Earth and Planetary Science Letters, v. 178, n. 3–4, p. 253–268, https://doi.org/10.1016/S0012-821X(00)00079-0

Hibbard, J. P., van Staal, C. R., Rankin, D. W., and Williams, H., 2006, Lithotectonic map of the Appalachian orogen, Canada-United States of America: Geological Survey of Canada, Map 2096A, 2 sheets, scale 1:1,500,000, https://doi.org/10.4095/221912

Jaffey, A. H., Flynn, K. F., Glendenin, L. E., Bentley, W. C., and Essling, A. M., 1971, Precision measurement of half-lives and specific activities of ^{235}U and ^{238}U: Physical Review, C4, p. 1889–1906, https://doi.org/10.1103/PhysRevC.4.1889

Jordan, B. T., Grunder, A. L., Duncan, R. A., and Deino, A. L., 2004, Geochronology of age-progressive volcanism of the Oregon High Lava Plains: Implications for the plume interpretation of Yellowstone: Journal of Geophysical Research-Solid Earth, v. 109, n. B10, p. B10202, https://doi.org/10.1029/2003JB002776

Kaislaniemi, L., and van Hunen, J., 2014, Dynamics of lithospheric thinning and mantle melting by edge-driven convection: Application to Moroccan Atlas mountains: Geochemistry, Geophysics, Geosystems, v. 15, n. 8, p. 3175–3189, https://doi.org/10.1002/2014GC005414

King, S. D., 2007, Hotspots and edge-driven convection: Geology, v. 35, n. 3, p. 223–226, https://doi.org/10.1130/G23291A.1

King, S. D., and Anderson, D. L., 1995, An alternative mechanism of flood basalt formation: Earth and Planetary Science Letters, v. 136, n. 3–4, p. 269–279, https://doi.org/10.1016/0012-821X(95)00205-Q

——— 1998, Edge-driven convection: Earth and Planetary Science Letters, v. 160, n. 3–4, p. 289–296, https://doi.org/10.1016/S0012-821X(98)00089-2

Kuiper, K. F., Deino, A., Hilgen, F. J., Krijgsman, W., Renne, P. R., and Wijbrans, A. J., 2008, Synchronizing rock clocks of Earth history: Science, v. 320, n. 5875, p. 500–504, https://doi.org/10.1126/science.1154339

Laurent, R., and Pierson, T. C., 1973, Petrology of alkaline rocks from Cuttingsville and the Shelburne Peninsula, Vermont: Canadian Journal of Earth Sciences, v. 10, n. 8, p. 1244–1256, https://doi.org/10.1139/e73-110

Lee, J. Y., Marti, K., Severinghaus, J. P., Kawamura, K., Yoo, H. S., Lee, J. B., and Kim, J. S., 2006, A redetermination of the isotopic abundances of atmospheric Ar: Geochimica et Cosmochimica Acta, v. 70, n. 17, p. 4507–4512, https://doi.org/10.1016/j.gca.2006.06.1563

Levin, V., Long, M. D., Skryzalin, P., Li, Y., and López, I., 2018, Seismic evidence for a recently formed mantle upwelling beneath New England: Geology, v. 46, n. 1, p. 87–90, https://doi.org/10.1130/G39641.1

Li, C., Gao, H., Williams, M. L., and Levin, V., 2018, Crustal thickness variation in the northern Appalachian mountains: Implications for the geometry of the 3-D tectonic boundaries within the crust: Geophysical Research Letters, v. 45, n. 12, p. 6061–6070, https://doi.org/10.1029/2018GL078777

Ludwig, K. R., 2003, Isoplot 3.00: A geochronological toolkit for Microsoft Excel: Berkeley, California, Berkeley Geochronology Center, 70 p.

Matton, G., and Jébrak, M., 2009, The Cretaceous Peri-Atlantic Alkaline Pulse (PAAP): Deep mantle plume origin or shallow lithospheric break-up?: Tectonophysics, v. 469, n. 1–4, p. 1–12, https://doi.org/10.1016/j.tecto.2009.01.001

Mazza, S. E., Gazel, E., Johnson, E. A., Kunk, M. J., McAleer, R., Spotila, J. A., Bizimis, M., and Coleman, D. S., 2014, Volcanoes of the passive margin: The youngest magmatic event in eastern North America: Geology, v. 42, n. 6, p. 483–486, https://doi.org/10.1130/G35407.1

Mazza, S. E., Gazel, E., Johnson, E. A., Bizimis, M., McAleer, R., and Biryol, C. B., 2017, Post-rift magmatic evolution of the eastern North American "passive-aggressive" margin: Geochemistry, Geophysics, Geosystems, v. 18, n. 1, p. 3–22, https://doi.org/10.1002/2016GC006646

McDougall, I., and Harrison, T. M., 1999, Geochronology and Thermochronology by the $^{40}Ar/^{39}Ar$ Method: Oxford, England, Oxford University Press, 269 p.

McEnroe, S. A., 1996, North America during the Lower Cretaceous: New paleomagnetic constraints from intrusions in New England: Geophysical Journal International, v. 126, n. 2, p. 477–494, https://doi.org/10.1111/j.1365-246X.1996.tb05304.x

McHone, J. G., 1978, Distribution, orientations, and ages of mafic dikes in central New England: GSA Bulletin, v. 89, n. 11, p. 1645–1655, https://doi.org/10.1130/0016-7606(1978)89<1645:DOAAOM>2.0.CO;2

——— 1984, Mesozoic igneous rocks of northern New England and adjacent Québec: Geological Society of America Map and Chart Series MC-49, scale 1:690,000, 1 sheet, 5 p. text.

——— 1996, Constraints on the mantle plume model for Mesozoic alkaline intrusions in northeastern North America: The Canadian Mineralogist, v. 34, p. 325–334.

McHone, J. G., and Butler, J. R., 1984, Mesozoic igneous provinces of New England and the opening of the North Atlantic Ocean: GSA Bulletin, v. 95, n. 7, p. 757–765, https://doi.org/10.1130/0016-7606(1984)95<757:MIPONE>2.0.CO;2

McHone, J. G., and Corneille, S. E., 1980, Alkalic dikes of the Lake Champlain Valley: Vermont Geology, v. 1, p. 16–21.

Menke, W., Skrylazin, P., Levin, V., Harper, T., Darbyshire, F., and Dong, T., 2016, The Northern Appalachian Anomaly: A modern asthenospheric upwelling: Geophysical Research Letters, v. 43, n. 19, p. 10,173–10,179, https://doi.org/10.1002/2016GL070918

Menke, W., Lamoureux, J., Abbott, D., Hopper, E., Hutson, D., and Marrero, A., 2018, Crustal heating and lithospheric erosion associated with asthenospheric upwelling beneath southern New England (USA): Journal of Geophysical Research–Solid Earth, v. 123, n. 10, p. 8995–9008, https://doi.org/10.1029/2018JB015921

Merle, R. E., Jourdan, F., Chiaradia, M., Olierook, H. K. H., and Manatschal, G., 2019, Origin of widespread Cretaceous alkaline magmatism in the Central Atlantic: A single melting anomaly?: Lithos, v. 342–343, p. 480–498, https://doi.org/10.1016/j.lithos.2019.06.002

Min, K., Mundil, R., Renne, P. R., and Ludwig, K. R., 2000, A test for systematic errors in $^{40}Ar/^{39}Ar$ geochronology through comparison with U/Pb analysis of a 1.1-Ga rhyolite: Geochimica et Cosmochimica Acta, v. 64, n. 1, p. 73–98, https://doi.org/10.1016/S0016-7037(99)00204-5

Morgan, W. J., 1972, Deep mantle convection plumes and plate motions: AAPG Bulletin, v. 56, n. 2, p. 203–213, https://doi.org/10.1306/819A3E50-16C5-11D7-8645000102C1865D

Müller, R. D., Seton, M., Zahirovic, S., Williams, S. E., Matthews, K. J., Wright, N. M., Shephard, G. E., Maloney, K. T., Barnett-Moore, N., Hosseinpour, M., Bower, D. J., and Cannon, J., 2016, Ocean basin evolution and global-scale plate reorganization events since Pangea breakup: Annual Review of Earth and Planetary Sciences, v. 44, p. 107–138, https://doi.org/10.1146/annurev-earth-060115-012211

Nebel, O., Scherer, E. S., and Mezger, K., 2011, Evaluation of the ^{87}Rb decay constant by age comparison against the U–Pb system: Earth and Planetary Science Letters, v. 301, n. 1–2, p. 1–8, https://doi.org/10.1016/j.epsl.2010.11.004

Philpotts, A. R., 1970, Mechanism of emplacement of the Monteregian intrusions: The Canadian Mineralogist, v. 10, n. 3, p. 395–410.

Praeg, D., Stoker, M. S., Shannon, P. M., Ceramicola, S., Hjelstuen, B., Laber, J. S., and Mathiesen, A., 2005, Episodic Cenozoic tectonism and the development of the NW "passive" continental margin: Marine and Petroleum Geology, v. 22, n. 9–10, p. 1007–1030, https://doi.org/10.1016/j.marpetgeo.2005.03.014

Ratcliffe, N. M., Stanley, R. S., Gale, M. H., Thompson, P. J., and Walsh, G. J., 2011, Bedrock geologic map of Vermont: U.S. Geological Survey Scientific Investigations Map 3184, 3 sheets, scale 1:100,000, https://doi.org/10.3133/sim3184

Renne, P. R., Mundil, R., Balco, G., Min, K., and Ludwig, K. R., 2010, Joint determination of ^{40}K decay constants and $^{40}Ar^*/^{40}K$ for the Fish Canyon sanidine standard, and improved accuracy for $^{40}Ar/^{39}Ar$ geochronology: Geochimica et Cosmochimica Acta, v. 74, n. 18, p. 5349–5367, https://doi.org/10.1016/j.gca.2010.06.017

Rondenay, S., Bostick, M. G., Hearn, T. M., White, D. J., and Mareschal, R. M., 2000, Lithospheric assembly and modification of the SE Canadian Shield: Abitibi-Grenville Teleseismic Experiment: Journal of Geophysical Research-Solid Earth, v. 105, n. B6, p. 13,735–13,754, https://doi.org/10.1029/2000JB900022

Roulleau, E., and Stevenson, R., 2013, Geochemical and isotopic (Nd–Sr–Hf–Pb) evidence for a lithospheric mantle source in the formation of the alkaline Monteregian province (Quebec): Canadian Journal of Earth Sciences, v. 50, n. 6, p. 650–666, https://doi.org/10.1139/cjes-2012-0145

Roulleau, E., Pinti, D. L., Stevenson, R. K., Takahata, N., Sano, Y., and Pitre, F., 2012, N, Ar and Pb isotopic co-variations in magmatic minerals: Discriminating fractionation processes from magmatic sources in Monteregian Hills, Québec, Canada: Chemical Geology, v. 326–327, p. 123–131, https://doi.org/10.1016/j.chemgeo.2012.07.016

Rutte, D., Becker, T. A., Deino, A. L., Reese, S. R., Renne, P. R., and Schlicker, R. A., 2018, The new CLOCIT irradiation facility for $^{40}Ar/^{39}Ar$ geochronology: Characterisation, comparison with CLICIT and implications for high-precision geochronology: Geostandards and Geoanalytical Research, v. 42, n. 3, p. 301–307, https://doi.org/10.1111/ggr.12217

Rychert, C. A., Fischer, K. M., and Rondenay, S., 2005, A sharp lithosphere-asthenosphere boundary imaged beneath eastern North America: Nature, v. 436, p. 542–545, https://doi.org/10.1038/nature03904

Rychert, C. A., Rondenay, S., and Fischer, K. M., 2007, *P*-to-*S* and *S*-to-*P* imaging of a sharp lithosphere-asthenosphere boundary beneath eastern North America: Journal of Geophysical Research-Solid Earth, v. 112, n. B8, p. B08314, https://doi.org/10.1029/2006JB004619

Shafiqullah, M., Tupper, W. M., and Cole, T. J. S., 1970, K–Ar age of the carbonatite complex, Oka, Quebec: The Canadian Mineralogist, v. 10, n. 3, p. 541–552.

Shen, W., and Ritzwoller, M. H., 2016, Crustal and uppermost mantle structure beneath the United States: Journal of Geophysical Research-Solid Earth, v. 121, n. 6, p. 4306–4342, https://doi.org/10.1002/2016JB012887

Sleep, N. H., 1990, Monteregian hotspot track: A long-lived mantle plume: Journal of Geophysical Research-Solid Earth, v. 95, n. B13, p. 21,983–21,990, https://doi.org/10.1029/JB095iB13p21983

Stoenner, R. W., Schaeffer, O. A., and Katcoff, S., 1965, Half-lives of argon-37, argon-39, and argon-42: Science, v. 148, n. 3675, p. 1325–1328, https://doi.org/10.1126/science.148.3675.1325

Thompson, R. N., and Gibson, S. A., 1991, Subcontinental mantle plumes, hotspots and pre-existing thin spots: Journal of the Geological Society, London, v. 148, n. 6, p. 973–977, https://doi.org/10.1144/gsjgs.148.6.0973

Wanless, R. K., Stevens, R. D., Lachance, G. R., and Delabio, R. N., 1973, K–Ar isotopic ages, Report 11: Geological Survey of Canada Paper 73-2, p. 75–77.

Withjack, M. O., Schlische, R. W., and Olsen, P. E., 2012, Development of the passive margin of eastern North America: Mesozoic rifting, igneous activity, and breakup, *in* Roberts, D. G., and Bally, A. W., editors, Regional Geology and Tectonics: Phanerozoic Rift Systems and Sedimentary Basins, p. 301–335, https://doi.org/10.1016/B978-0-444-56356-9.00012-2

Zartman, R. E., Brock, M. R., Heyl, A. V., and Thomas, H. H., 1967, K–Ar and Rb–Sr ages of some alkalic intrusive rocks from central and eastern United States: American Journal of Science, v. 265, n. 10, p. 848–870, https://doi.org/10.2475/ajs.265.10.848

Zen, E-An, 1972, Some revisions in the interpretation of the Taconic allochthon in west-central Vermont: GSA Bulletin, v. 83, n. 9, p. 2573–2588, https://doi.org/10.1130/0016-7606(1972)83[2573:SRITIO]2.0.CO;2